

# **Modeling Solvent Effects in Optical Lithography**

by

Chris A. Mack

Copyright 1998 by Chris Alan Mack

**Modeling Solvent Effects in  
Optical Lithography**

by

**Chris Alan Mack, B.S., M.S.**

**Dissertation**

Presented to the Faculty of the Graduate School of  
the University of Texas at Austin  
in Partial Fulfillment  
of the Requirements  
for the Degree of  
Doctor of Philosophy

The University of Texas at Austin

December 1998

### *Acknowledgements*

I would like to thank Kathi Mueller and Allen Gardiner for providing the experimental data used for this study, and for many helpful discussions. I would also like to thank Dr. C. Grant Willson for his insight and guidance throughout this work and Dr. Isaac Trachtenberg for his continuous support.

# **Modeling Solvent Effects in Optical Lithography**

Publication No. \_\_\_\_\_

Chris Alan Mack, PhD

The University of Texas at Austin, 1998

Supervisor: Isaac Trachtenberg

A theoretical and experimental study into the effects of residual casting solvent on the lithographic properties of photoresist films is described. A modification to the common Fujita-Doolittle equation is proposed which provides an accurate description of the temperature and concentration dependence of solvent diffusivity in polymer systems. This model, in combination with a variable grid, finite difference time domain numerical solution to the diffusion equation, allows for calculation of the residual casting solvent content as a function of bake conditions. Using measurements of solvent content of a commercial i-line photoresist after post apply bake from a quartz crystal microbalance and radio-labeled solvent with scintillation counting, the model was verified. Analysis of this data has led to a calibrated model of solvent diffusivity as a function of solvent content and bake temperature, which can then predict solvent content as a function of depth into the photoresist for any bake conditions.

# Chapter 1

## Introduction

Optical lithography has been, and continues to be, one of the major driving forces behind the remarkable advances in semiconductor technology over the last 30 years. The reduction in the minimum resolvable feature size printed onto a silicon wafer has led to smaller, faster, cheaper transistors that are connected together into ever more powerful integrated circuits. Historically, the minimum feature size used in the mass production of these integrated circuits has been reduced by a factor of two every six years [1.1]. This incredibly reliable improvement comes from continuous improvement of the tools and materials used in lithographic processing, and from our improved understanding of the theory of lithographic science.

One important tool over the years for understanding lithography is simulation [1.2]. Lithography models based on the physics and chemistry of the lithography process allow complex calculations to be carried out quickly and easily. These simulation tools provide “virtual” experiments that otherwise might be too expensive or difficult or time consuming to be practical. Optical lithography simulation enables researchers to investigate new approaches to imaging, gives process development engineers a convenient tool for designing and optimizing new processes, and provides essential expert information for manufacturing problem solving.

A key to the success of lithography simulation is its firm foundation in the physical principles of lithography. In essence, a lithography model is nothing more than the theory of lithography embedded in software code. Thus, simulating a process involves first understanding the fundamental concepts underlying that process. The better the understanding, the better the model. One area of lithography simulation that has remained weak is the modeling of the thermal processing of photoresist, in particular the post apply bake.

Thermal processing of photoresists (post apply bake and post exposure bake) can dramatically influence resist performance in a number of ways. It is well known that residual solvent has a powerful influence on the dissolution rate of thin polymer films [1.3,1.4] and that post apply bake (PAB) determines the resist’s residual solvent content [1.8-1.9]. However, quantitative determination of the influence of bake conditions on residual solvent is still lacking. This study establishes a lithographic model for the effect of PAB on solvent content and distribution that is based on fundamental and measurable physical properties. The availability of such a model will be a valuable tool for both resist designers and lithographic process engineers.

This thesis is organized as follows: Chapter 2 provides an overview of lithographic modeling. Chapters 3, 4, and 5 give detailed descriptions of the exposure, bake and development models, respectively, in use today. Chapter 6 reviews past efforts at modeling solvent diffusion in polymer systems and proposes a new model. Chapter 7 uses this new model to match experimental data and to extract the solvent diffusion modeling parameters for a specific commercial resist system.

## References

- 1.1 C. A. Mack, "Trends in Optical Lithography," *Optics and Photonics News* (April, 1996) pp. 29-33.
- 1.2 C. A. Mack, Inside PROLITH: A Comprehensive Guide to Optical Lithography Simulation, FINLE Technologies (Austin, TX: 1997).
- 1.3 A. C. Ouano, "Dependence of Dissolution Rate on Processing and Molecular Parameters of Resists," *Polymers in Electronics*, ACS Vol. 242 (1984) pp. 79-90.
- 1.4 B. T. Beauchemin, C. E. Ebersole, and I. Daraktchiev, "The Influence of Absorbed Solvent on Novolak and Resist Film Dissolution and Thermal Behavior," *Advances in Resist Technology and Processing XI, Proc.*, SPIE Vol. 2195 (1994) pp. 610-623.
- 1.5 C. A. Mack, D. P. DeWitt, B. K. Tsai, and G. Yetter, "Modeling of Solvent Evaporation Effects for Hot Plate Baking of Photoresist," *Advances in Resist Technology and Processing XI, Proc.*, SPIE Vol. 2195 (1994) pp. 584-595.
- 1.6 C.A. Mack, K.E. Mueller, A.B. Gardiner, A. Qiu, R.R. Dammel, W.G. Koros, C.G. Willson, "Diffusivity Measurements in Polymers, Part 1: Lithographic Modeling Results," *Advances in Resist Technology and Processing XIV, Proc.*, SPIE Vol. 3049 (1997) pp. 355-362.
- 1.7 Allen B. Gardiner, Anwei Qin, Clifford L. Henderson, William J. Koros, C. Grant Willson, Ralph R. Dammel, Chris Mack, William D. Hinsberg, "Diffusivity Measurements in Polymers, Part 2: Residual Casting Solvent Measurement by Liquid Scintillation Counting," *Advances in Resist Technology and Processing XIV, Proc.*, SPIE Vol. 3049 (1997) pp. 850-860.
- 1.8 K. E. Mueller, W. J. Koros, Y. Y. Wang, and C. G. Willson, "Diffusivity Measurements in Polymers, Part 3: Quartz Crystal Microbalance Techniques," *Advances in Resist Technology and Processing XIV, Proc.*, SPIE Vol. 3049 (1997) pp. 871-878.
- 1.9 Katherine E. Mueller, William J. Koros, Chris A. Mack, C.G. Willson, "Diffusivity Measurements in Polymers, Part 4: Acid Diffusion in Chemically Amplified Resists," *Advances in Resist Technology and Processing XIV, Proc.*, SPIE Vol. 3049 (1997) pp. 706-711.

# Chapter 2

## Optical Lithography Simulation

Optical lithography modeling began in the early 1970s when Rick Dill and coworkers started an effort at IBM Thomas J. Watson Research Center in Yorktown Heights, NY to describe the basic steps of the lithography process with mathematical equations. At a time when lithography was considered a true art, such an approach was met with much skepticism. The results of their pioneering work were published in a landmark series of papers in 1975 [2.1-2.4], now referred to as the “Dill papers.” These papers not only gave birth to the field of lithography modeling, they represented the first serious attempt to describe lithography not as an art, but as a science. These papers presented a simple model for image formation with incoherent illumination, the first order kinetic “Dill model” of exposure, and an empirical model for development coupled with a cell algorithm for photoresist profile calculation. The Dill papers are still the most referenced works in the body of lithography literature.

While Dill’s group worked on the beginnings of lithography simulation, a professor from the University of California at Berkeley, Andy Neureuther, spent a year on sabbatical working with Dill. Upon returning to Berkeley, Neureuther and another professor, Bill Oldham, started their own modeling effort. In 1979 they presented the first result of their effort, the lithography modeling program SAMPLE [2.5]. SAMPLE improved the state of the art in lithography modeling by adding partial coherence to the image calculations and by replacing the cell algorithm for dissolution calculations with a string algorithm. But more importantly, SAMPLE was made available to the lithography community. For the first time, researchers in the field could use modeling as a tool to help understand and improve their lithography processes.

My work in the area of lithographic simulation began in 1983, and in 1985 I introduced the model PROLITH (the Positive Resist Optical LITHography model) [2.6]. This model added an analytical expression for the standing wave intensity in the resist, a prebake model, a new kinetic model for resist development, and the first model for contact and proximity printing. PROLITH was also the first lithography simulator to run on a personal computer (the IBM PC), making lithography modeling accessible to all lithographers, from advanced researchers to process development engineers to manufacturing engineers. Over the years, PROLITH advanced to include a model for contrast enhancement materials, the extended source method for partially coherent image calculations, and an advanced focus model for high numerical aperture imaging.

Figure 2-1 shows a basic schematic of the calculation steps required for lithography modeling. A brief overview of the physical models found in most lithography simulation programs is provided below. More details on some of these models can be found in subsequent chapters.

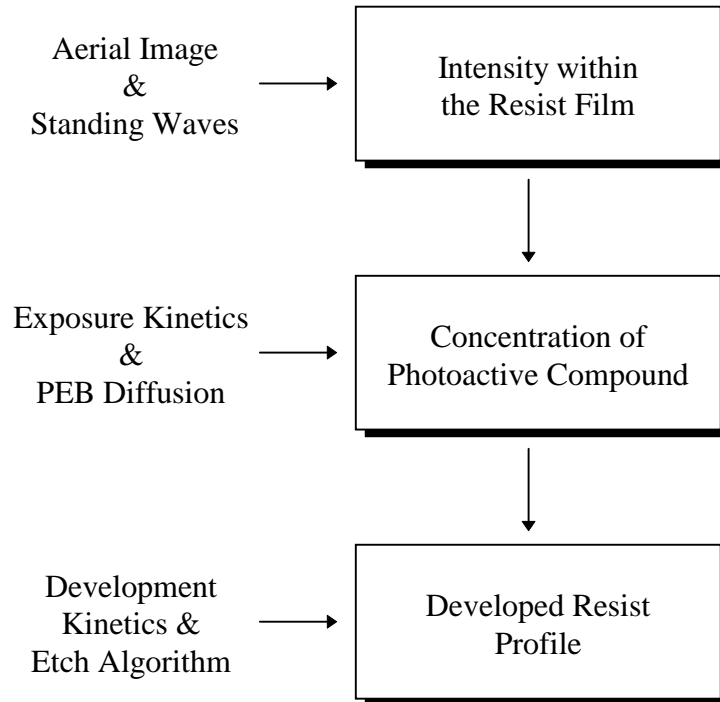


Figure 2-1. Flow diagram of a lithography model.

**Aerial Image:** The extended source method is used to predict the aerial image of a partially coherent diffraction limited or aberrated projection system based on scalar and/or vector diffraction theory. Single wavelength or broadband illumination can be used. The standard image model accounts for the important effect of image defocus through the resist film. Mask patterns can be one-dimensional lines and spaces or small two dimensional contacts and islands. Phase-shifting masks and off-axis illumination can be simulated and pupil filters can be defined.

**Standing Waves:** An analytical expression is used to calculate the standing wave intensity as a function of depth into the resist, including the effects of resist bleaching, on planar substrates. Contrast enhancement layers or top-layer anti-reflection coatings can also be included. High numerical aperture models include the effects of non-vertical light propagation.

**Prebake:** Thermal decomposition of the photoresist photoactive compound during prebake (also called post apply bake) is modeled using first order kinetics resulting in a change in the resist's optical properties. Many important bake effects, however, are not yet well understood. It is the purpose of this work to enhance the state-of-the-art in prebake modeling by predicting the influence of bake conditions on the solvent distribution and content that results.

**Exposure:** First order kinetics are used to model the chemistry of exposure. Both positive and negative resists can be simulated.

**Post-Exposure Bake:** A two-dimensional or three-dimensional diffusion calculation allows the post-exposure bake to reduce the effects of standing waves. For chemically amplified resists, this diffusion is accompanied by an amplification reaction which accounts for crosslinking, blocking, or deblocking in an acid catalyzed reaction. Acid loss mechanisms and non-constant diffusivity can also be simulated.

**Development:** Kinetic models for resist dissolution are used in conjunction with an etching algorithm to determine the resist profile. Surface inhibition or enhancement can also be taken into account.

The combination of the models described above provides a complete mathematical description of the optical lithography process. Use of the models incorporated in a full lithography simulation package allows the user to investigate many interesting and important aspects of optical lithography.

## References

- 2.1 F. H. Dill, "Optical Lithography," *IEEE Trans. Electron Devices*, ED-22, No. 7 (1975) pp. 440-444.
- 2.2 F. H. Dill, W. P. Hornberger, P. S. Hauge, and J. M. Shaw, "Characterization of Positive Photoresist," *IEEE Trans. Electron Devices*, ED-22, No. 7 (July, 1975) pp. 445-452.
- 2.3 K. L. Konnerth and F. H. Dill, "In-Situ Measurement of Dielectric Thickness During Etching or Developing Processes," *IEEE Trans. Electron Devices*, ED-22, No. 7 (1975) pp. 452-456.
- 2.4 F. H. Dill, A. R. Neureuther, J. A. Tuttle, and E. J. Walker "Modeling Projection Printing of Positive Photoresists," *IEEE Trans. Electron Devices*, ED-22, No. 7 (1975) pp. 456-464.
- 2.5 W. G. Oldham, S. N. Nandgaonkar, A. R. Neureuther and M. O'Toole, "A General Simulator for VLSI Lithography and Etching Processes: Part I - Application to Projection Lithography," *IEEE Trans. Electron Devices*, ED-26, No. 4 (April, 1979) pp. 717-722.
- 2.6 C. A. Mack, "PROLITH: A Comprehensive Optical Lithography Model," *Optical Microlithography IV, Proc.*, SPIE Vol. 538 (1985) pp. 207-220.

# Chapter 3

## Photoresist Exposure Kinetics

The kinetics of photoresist exposure is intimately tied to the phenomenon of absorption. The discussion below begins with a description of absorption, followed by the chemical kinetics of exposure. Next, the chemistry of chemically amplified resists is reviewed. Finally, a description of the measurement method for the kinetic exposure parameters is given.

### A. Absorption

The phenomenon of absorption can be viewed on a macroscopic or a microscopic scale. On the macro level, absorption is described by the familiar Lambert and Beer laws, which give a linear relationship between absorbance and path length times the concentration of the absorbing species. On the micro level, a photon is absorbed by an atom or molecule, promoting an electron to a higher energy state. Both methods of analysis yield useful information needed in describing the effects of light on a photoresist.

The basic law of absorption is an empirical one. It was first expressed by Lambert (circa 1760) and can be expressed in differential form as

$$\frac{dI}{dz} = -\alpha I \quad (3.1)$$

where  $I$  is the intensity of light traveling in the  $z$ -direction through a medium, and  $\alpha$  is the absorption coefficient of the medium and has units of inverse length. This law is basically a single photon absorption probability equation: the probability that a photon will be absorbed is proportional to the photon flux. In a homogeneous medium (i.e.,  $\alpha$  is not a function of  $z$ ), equation (3.1) may be integrated to yield

$$I(z) = I_0 \exp(-\alpha z) \quad (3.2)$$

where  $z$  is the distance the light has traveled through the medium and  $I_0$  is the intensity at  $z = 0$ . If the medium is inhomogeneous, equation (3.2) becomes

$$I(z) = I_0 \exp(-Abs(z)) \quad (3.3)$$

where

$$Abs(z) = \int_0^z \alpha(z') dz' = \text{the absorbance}$$

When working with electromagnetic radiation, it is often convenient to describe the radiation by its complex electric field vector. The propagation of an electric field through some material can implicitly account for absorption by using a complex index of refraction  $\mathbf{n}$  for the material such that

$$\mathbf{n} = n - i\kappa \quad (3.4)$$

The imaginary part of the index of refraction is related to the absorption coefficient by

$$\alpha = 4\pi\kappa/\lambda \quad (3.5)$$

Note that the sign of the imaginary part of the index in equation (3.4) depends on the sign convention chosen for the phasor representation of the electric field. For typical absorption calculations in thin films, the “standard” sign convention most commonly used in the literature results in a negative imaginary part of the index of refraction. If the wrong sign is chosen in equation (3.4), the material will amplify the electric field rather than absorb it.

In 1852, August Beer showed that for dilute solutions the absorption coefficient is proportional to the concentration of the absorbing species in the solution.

$$\alpha_{\text{solution}} = ac \quad (3.6)$$

where  $a$  is the molar absorption coefficient (sometimes called the extinction coefficient) of the absorbing species (given by  $a = \alpha_0 MW/\rho$ , where  $\alpha_0$  is the absorption coefficient of the pure material,  $MW$  is the molecular weight,  $\rho$  is the density) and  $c$  is the concentration. The stipulation that the solution be dilute expresses a fundamental limitation of Beer's law. At high concentrations, where absorbing molecules are close together, the absorption of a photon by one molecule may be affected by a nearby molecule [3.1]. Since this interaction is concentration dependent, it causes deviation from the linear relation (3.6). Also, an apparent deviation from Beer's law occurs if the real part of the index of refraction changes appreciably with concentration. Thus, the validity of Beer's law should always be verified over the concentration range of interest.

For an  $N$  component homogeneous solid, the overall absorption coefficient becomes

$$\alpha_T = \sum_{j=1}^N a_j c_j \quad (3.7)$$

The linear addition of absorption terms presumes that Beer's law holds across components, i.e., that the absorption by one material is not influenced by the presence of the other materials. Of the total amount of light absorbed, the fraction of light which is absorbed by component  $i$  is given by

$$\frac{I_{Ai}}{I_{AT}} = \frac{a_i c_i}{\alpha_T} \quad (3.8)$$

where  $I_{AT}$  is the total light absorbed by the film, and  $I_{Ai}$  is the light absorbed by component  $i$ .

The concepts of macroscopic absorption will now be applied to a typical positive photoresist. A diazonaphthoquinone positive photoresist is made up of four major components; a base resin  $R$  that gives the resist its structural properties, a photoactive compound  $M$  (abbreviated PAC, this is the light sensitive moiety in the resist), exposure products  $P$  generated by the reaction of  $M$  with ultraviolet light, and a solvent  $S$ . Although photoresist drying during prebake is intended to drive off solvents, thermal studies have shown that a resist may contain up to 10% solvent after a typical prebake [3.2, 3.3]. The absorption coefficient  $\alpha$  is then

$$\alpha = a_M M + a_P P + a_R R + a_S S \quad (3.9)$$

If  $M_o$  is the initial PAC concentration (i.e., with no UV exposure), the stoichiometry of the exposure reaction gives

$$P = M_o - M \quad (3.10)$$

Equation (3.9) may be rewritten as [3.4]

$$\alpha = Am + B \quad (3.11)$$

where  $A = (a_M - a_P)M_o$   
 $B = a_P M_o + a_R R + a_S S$   
 $m = M/M_o$

$A$  and  $B$  are called the bleachable and non-bleachable absorption coefficients, respectively, and make up the first two Dill photoresist parameters [3.4]. Other non-bleachable components of the photoresist (such as a dye additive) are added to the  $B$  term above.

The quantities  $A$  and  $B$  are experimentally measurable [3.4] and can be easily related to typical resist absorbance curves, measured using a UV spectrophotometer. When the resist is fully exposed,  $M = 0$  and

$$\alpha_{exposed} = B \quad (3.12)$$

Similarly, when the resist is unexposed,  $m = 1$  ( $M = M_o$ ) and

$$\alpha_{unexposed} = A + B \quad (3.13)$$

From this  $A$  may be found by

$$A = \alpha_{unexposed} - \alpha_{exposed} \quad (3.14)$$

Thus,  $A(\lambda)$  and  $B(\lambda)$  may be determined from the UV absorbance curves of unexposed and completely exposed resist (Figure 3-1). A more complete description of the measurement of  $A$  and  $B$  is given in a following section.

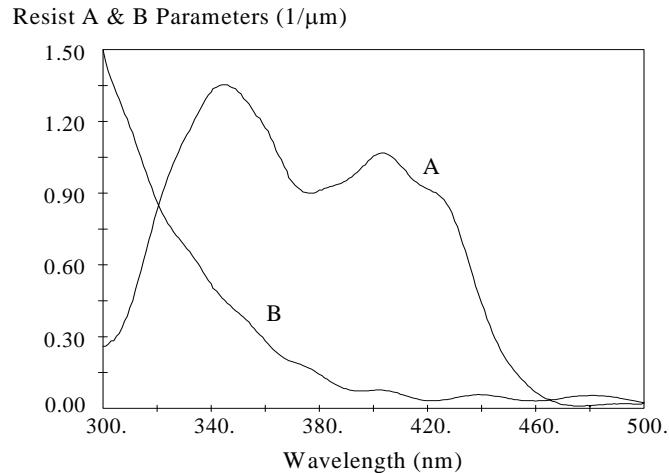


Figure 3-1. Resist parameters  $A$  and  $B$  as a function of wavelength measured with a UV spectrophotometer for a typical g-line resist.

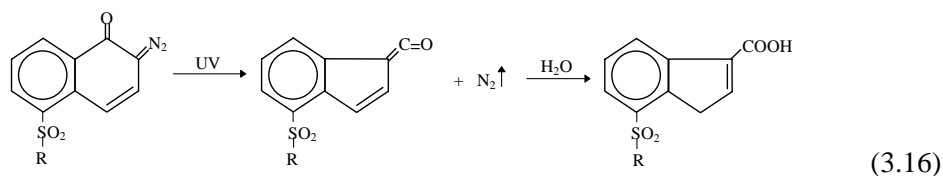
As mentioned previously, Beer's law is empirical in nature and, thus, should be verified experimentally. In the case of positive photoresists, this means formulating resist mixtures with differing photoactive compound to resin ratios and measuring the resulting  $A$  parameters. Previous work has shown that Beer's law is valid for conventional photoresists over the full practical range of PAC concentrations [3.5].

## B. Exposure Kinetics

On a microscopic level, the absorption process can be thought of as photons being absorbed by an atom or molecule causing an outer electron to be promoted to a higher energy state. This phenomenon is especially important for the photoactive compound since it is the absorption of UV light that leads to the chemical conversion of  $M$  to  $P$ .



This concept is stated in the first law of photochemistry: only the light that is absorbed by a molecule can be effective in producing photochemical change in the molecule. The actual chemistry of diazonaphthoquinone exposure is given below [3.6]:



The chemical reaction (3.15) can be rewritten in a more general form as



where  $M$  is the photoactive compound (PAC),  $M^*$  is the PAC molecule in an excited state,  $P$  is the carboxylic acid (product), and  $k_1, k_2, k_3$  are the rate constants for each reaction. Simple kinetics can now be applied. The proposed mechanism (3.17) assumes that all reactions are first order. Thus, the rate equation for each species can be written.

$$\begin{aligned} \frac{dM}{dt} &= k_2 M^* - k_1 M \\ \frac{dM^*}{dt} &= k_1 M - (k_2 + k_3) M^* \\ \frac{dP}{dt} &= k_3 M^* \end{aligned} \quad (3.18)$$

A system of three coupled linear first order differential equations can be solved exactly using Laplace transforms and the initial conditions [3.7]

$$\begin{aligned} M(t=0) &= M_o \\ M^*(t=0) &= P(t=0) = 0 \end{aligned} \quad (3.19)$$

However, if one uses the steady state approximation the solution becomes much simpler. This approximation assumes that in a very short time the excited molecule  $M^*$  comes to a steady state, i.e.,  $M^*$  is formed as quickly as it disappears. In mathematical form,

$$\frac{dM^*}{dt} = 0 \quad (3.20)$$

A previous study has shown that  $M^*$  does indeed come to a steady state quickly, on the order of  $10^{-8}$  seconds or faster [3.7]. Thus,

$$\frac{dM}{dt} = -KM \quad (3.21)$$

where

$$K = \frac{k_1 k_3}{k_2 + k_3}$$

Assuming  $K$  remains constant with time (an assumption we shall soon dispose of),

$$M = M_o \exp(-Kt) \quad (3.22)$$

The overall rate constant  $K$  is a function of the intensity of the exposure radiation. An analysis of the microscopic absorption of a photon predicts that  $K$  is directly proportional to the intensity of the exposing radiation [3.5]. The rate constant  $k_1$  in equation (3.17) will be proportional to the rate of photon absorption, which in turn is proportional to the photon flux (by Lambert's law) and thus the intensity. A more useful form of equation (3.21) is then

$$\frac{dm}{dt} = -CIm \quad (3.23)$$

where the relative PAC concentration  $m (= M/M_o)$  has been used and  $C$  is the standard exposure rate constant and the third Dill photoresist parameter [3.4].

A solution to the exposure rate equation (3.23) is simple if the intensity within the resist is constant throughout the exposure. However, this is generally not the case. In fact, many resists *bleach* upon exposure, that is, they become more transparent as the photoactive compound  $M$  is converted to product  $P$ . This corresponds to a positive value of  $A$ , as seen, for example, in Figure 3-1. Since the intensity varies as a function of exposure time, this variation must be known in order to solve the exposure rate equation. In the simplest possible case, a resist film coated on a substrate of the same index of refraction, only absorption affects the intensity within the resist. Thus, Lambert's law of absorption, coupled with Beer's law, could be applied.

$$\frac{dI}{dz} = -(Am + B)I \quad (3.24)$$

where equation (3.11) was used to relate the absorption coefficient to the relative PAC concentration. Equations (3.23) and (3.24) are coupled, and thus become first order non-linear partial differential equations which must be solved simultaneously. The solution to equations (3.23) and (3.24) was first carried out numerically for the case of lithography simulation [3.4], but in fact was solved analytically by Herrick [3.8] many years earlier. The same solution was also presented more recently by Diamond and Sheats [3.9] and by Babu and Barouch [3.10]. These solutions take the form of a single numerical integration, which is much simpler than solving two differential equations!

Although an analytical solution exists for the simple problem of exposure with absorption only, in more realistic problems the variation of intensity with depth in the film is more complicated than equation (3.24). In fact, the general exposure situation results in the formation of standing waves. In such a case, equations (4.1) - (4.4) can give the intensity within the resist as a function of the PAC distribution  $m(x,y,z,t)$ . Initially, this distribution is simply  $m(x,y,z,0) = 1$  (resulting in a uniform index of refraction). Thus, equation (4.1), for example, would give  $I(x,y,z,0)$ . The exposure equation (3.23) can then be integrated over a small increment of exposure time  $\Delta t$  to produce the PAC distribution  $m(x,y,z,\Delta t)$ .

The assumption is that over this small increment in exposure time the intensity remains relatively constant, leading to the exponential solution

$$m(x, y, z, t + \Delta t) = m(x, y, z, t) \exp(-CI\Delta t) \quad (3.25)$$

This new PAC distribution is then used to calculate the new intensity distribution  $I(x, y, z, \Delta t)$ , which in turn is used to generate the PAC distribution at the next increment of exposure time  $m(x, y, z, 2\Delta t)$ . This process continues until the final exposure time is reached.

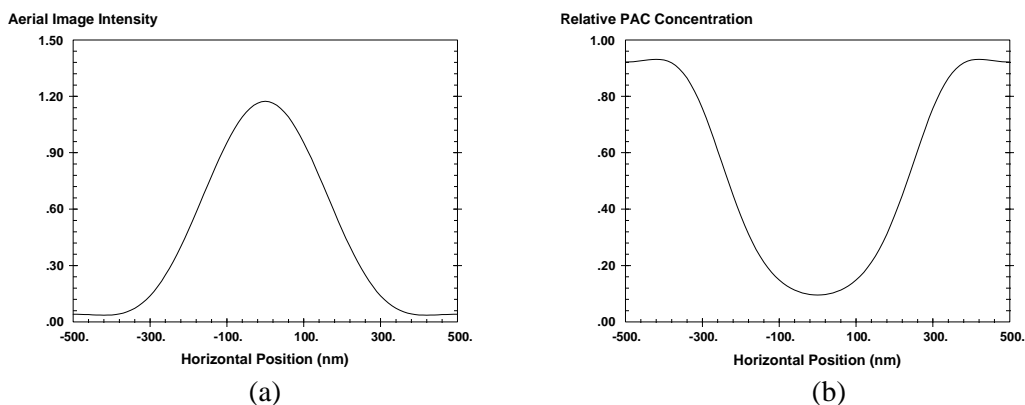
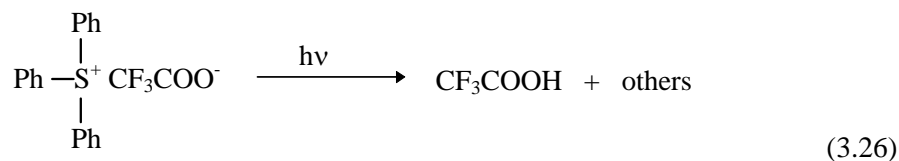


Figure 3-2. The exposure process takes an aerial image (a) and converts it into a latent image (b), shown at a given depth into the photoresist.

The final result of exposure is the conversion of an aerial image  $I(x, y, z)$  into a latent image  $m(x, y, z)$ . Figure 3-2 illustrates a one-dimensional case.

### C. Chemically Amplified Resists

Chemically amplified photoresists are composed of a polymer resin (possibly “blocked” to inhibit dissolution), a photoacid generator (PAG), and possibly a crosslinking agent, dye or other additive. As the name implies, the photoacid generator forms a strong acid when exposed to Deep-UV light. Ito and Willson first proposed the use of an aryl onium salt [3.11], and triphenylsulfonium salts have been studied extensively as PAGs. The reaction of a common PAG is shown below:



The acid generated in this case (trifluoroacetic acid) is a derivative of acetic acid where the electron-drawing properties of the fluorines are used to greatly increase the acidity of the molecule. The PAG is

mixed with the polymer resin at a concentration of typically 2-15% by weight, with 5-10% as typical formulations.

The kinetics of the exposure reaction are presumed to be standard first order:

$$\frac{\partial G}{\partial t} = -CIG \quad (3.27)$$

where  $G$  is the concentration of PAG at time  $t$  (the initial PAG concentration is  $G_o$ ),  $I$  is the exposure intensity, and  $C$  is the exposure rate constant. For constant intensity, the rate equation can be solved for  $G$ :

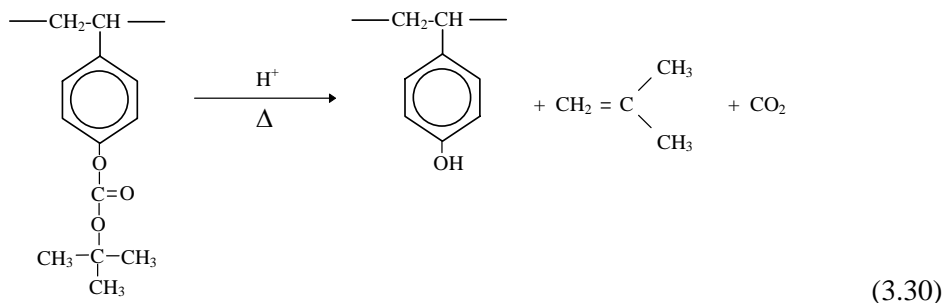
$$G = G_o e^{-CIt} \quad (3.28)$$

The acid concentration  $H$  is given by

$$H = G_o - G = G_o (1 - e^{-CIt}) \quad (3.29)$$

If the intensity is not constant throughout the exposure, then the iterative approach described in the section above can certainly be used.

Exposure of the resist with an aerial image  $I(x)$  results in an acid latent image  $H(x)$ . A post-exposure bake (PEB) is then used to thermally induce a chemical reaction. This may be the activation of a crosslinking agent for a negative resist or the deblocking of the polymer resin for a positive resist. The reaction is catalyzed by the acid so that the acid is not consumed by the reaction and, to first order,  $H$  remains constant. Ito and Willson first proposed the concept of deblocking a polymer to change its solubility [3.11]. A base polymer such as polyhydroxystyrene, PHS, is used which is very soluble in an aqueous base developer. It is the hydroxyl groups which give the PHS its high solubility, so by "blocking" these sites (by reacting the hydroxyl group with some longer chain molecule) the solubility can be reduced. Ito and Willson employed a *t*-butoxycarbonyl group (*t*-BOC), resulting in a very slowly dissolving polymer. In the presence of acid (which acts as a catalyst) and heat, the *t*-BOC blocked polymer will undergo acidolysis to generate the soluble hydroxyl group, as shown below.



One drawback of this scheme is that the cleaved *t*-BOC is volatile and will evaporate, causing film shrinkage in the exposed areas. Larger molecular weight blocking groups can be used to reduce this

film shrinkage to acceptable levels (below 10%). Also, the blocking group is such an effective inhibitor of dissolution that nearly every blocked site on the polymer must be deblocked in order to obtain significant dissolution. Thus, the photoresist can be made more “sensitive” by only partially blocking the PHS. Typical photoresists use 10-30% of the hydroxyl groups blocked, with 20% a typical value. Molecular weights for the PHS run in the range of 3000 to 5000 giving about 20 to 35 hydroxyl groups per polymer molecule, about 4 to 7 of which are initially blocked.

Using  $M$  as the concentration of some reactive site, these sites are consumed (i.e., are reacted) according to kinetics of some unknown order in  $H$  and first order in  $M$  [3.12]:

$$\frac{\partial M}{\partial t'} = -K_{amp} M H^n \quad (3.31)$$

where  $K_{amp}$  is the rate constant of the amplification reaction (crosslinking, deblocking, etc.) and  $t'$  is the bake time. Simple theory would indicate that  $n = 1$ , but the general form will be used here. Assuming  $H$  is constant, equation (3.31) can be solved for the concentration of reacted sites  $X$ :

$$X = M_o - M = M_o \left(1 - e^{-K_{amp} H^n t'}\right) \quad (3.32)$$

(Note: Although  $H^+$  is not consumed by the reaction, the value of  $H$  is not locally constant. Diffusion during the PEB and acid loss mechanisms cause local changes in the acid concentration, thus requiring the use of a reaction-diffusion system of equations. The approximation that  $H$  is constant is a useful one, however, which gives insight into the reaction as well as accurate results under some conditions.)

It is useful here to normalize the concentrations to some initial values. This results in a normalized acid concentration  $h$  and normalized reacted and unreacted sites  $x$  and  $m$ :

$$h = \frac{H}{G_o} \quad x = \frac{X}{M_o} \quad m = \frac{M}{M_o} \quad (3.33)$$

Equations (3.30) and (3.32) become

$$\begin{aligned} h &= 1 - e^{-CIt} \\ m &= 1 - x = e^{-\alpha h^n} \end{aligned} \quad (3.34)$$

where  $\alpha$  is a lumped “amplification” constant equal to  $G_o^n K_{amp} t'$ . The result of the PEB is an amplified latent image  $m(x)$ , corresponding to an exposed latent image  $h(x)$ , resulting from the aerial image  $I(x)$ .

The above analysis of the kinetics of the amplification reaction assumed a locally constant concentration of acid  $H$ . Although this could be exactly true in some circumstances, it is typically only an approximation, and is often a poor approximation. In reality, the acid diffuses during the bake. In one dimension, the standard diffusion equation takes the form

$$\frac{\partial H}{\partial t'} = \frac{\partial}{\partial z} \left( D_H \frac{\partial H}{\partial z} \right) \quad (3.35)$$

where  $D_H$  is the diffusivity of acid in the photoresist. Solving this equation requires a number of things: two boundary conditions for each dimension, one initial condition, and a knowledge of the diffusivity as a function of position and time.

The initial condition is the initial acid distribution within the film,  $H(x,y,z,0)$ , resulting from the exposure of the PAG. The two boundary conditions are at the top and bottom surface of the photoresist film. The boundary at the wafer surface is assumed to be impermeable, giving a boundary condition of no diffusion into the wafer. The boundary condition at the top of the photoresist will depend on the diffusion of acid into the atmosphere above the wafer, as described below. In the plane of the wafer (x- and y-directions), boundary conditions will depend on the geometry of the problem.

The solution of equation (3.35) can now be performed if the diffusivity of the acid in the photoresist is known. Unfortunately, this solution is complicated by two very important factors: the diffusivity is a strong function of temperature and, most probably, the extent of amplification. Since the temperature is changing with time during the bake, the diffusivity will be time dependent. The concentration dependence of diffusivity results from an increase in free volume for typical positive resists: as the amplification reaction proceeds, the polymer blocking group evaporates resulting in a decrease in film thickness but also an increase in free volume (and probably a change in the glass transition temperature as well). Since the acid concentration is time and position dependent, the diffusivity in equation (3.35) must be determined as a part of the solution of equation (3.35) by an iterative method. The resulting simultaneous solution of equations (3.31) and (3.35) is called a *reaction-diffusion* system.

The temperature dependence of the diffusivity can be expressed in a standard Arrhenius form:

$$D_o(T) = A_r \exp(-E_a / RT) \quad (3.36)$$

where  $D_o$  is a general diffusivity,  $A_r$  is the Arrhenius coefficient,  $E_a$  is the activation energy,  $R$  is the universal gas constant, and  $T$  is the absolute temperature. A full treatment of the amplification reaction would include a thermal model of the hotplate in order to determine the actual time-temperature history of the wafer [3.13]. To simplify the problem, an ideal temperature distribution will be assumed -- the temperature of the resist is zero (low enough for no diffusion or reaction) until the start of the bake, at which time it immediately rises to the final bake temperature, stays constant for the duration of the bake, then instantly falls back to zero.

The concentration dependence of the diffusivity is less obvious. Several authors have proposed and verified the use of different models for the concentration dependence of diffusion within a polymer. Of course, the simplest form (besides a constant diffusivity) would be a linear model. Letting  $D_o$  be the diffusivity of acid in completely unreacted resist and  $D_f$  the diffusivity of acid in resist which has been completely reacted,

$$D_H = D_o + x(D_f - D_o) \quad (3.37)$$

Here, diffusivity is expressed as a function of the extent of the amplification reaction  $x$ . Another common form is the Fujita-Doolittle equation [3.14] which can be predicted theoretically using free volume arguments. A form of that equation which is convenient for calculations is shown here:

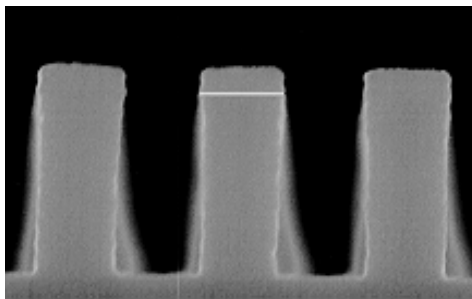
$$D_H = D_o \exp\left(\frac{\alpha x}{1 + \beta x}\right) \quad (3.38)$$

where  $\alpha$  and  $\beta$  are experimentally determined constants. Other concentration relationships are also possible [3.15].

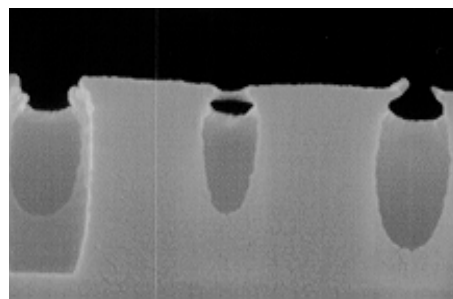
Through a variety of mechanisms, acid formed by exposure of the resist film can be lost and thus not contribute to the catalyzed reaction to change the resist solubility. There are two basic types of acid loss: loss that occurs between exposure and post-exposure bake, and loss that occurs during the post-exposure bake. The first type of loss leads to delay time effects -- the resulting lithography is affected by the delay time between exposure and post-exposure bake. Delay time effects can be very severe and, of course, are very detrimental to the use of such a resist in a manufacturing environment [3.16, 3.17]. The typical mechanism for delay time acid loss is the diffusion of atmospheric base contaminants into the top surface of the resist. The result is a neutralization of the acid near the top of the resist and a corresponding reduced amplification. For a negative resist, the top portion of a line is not insolubilized and resist is lost from the top of the line. For a positive resist, the effects are more devastating. Sufficient base contamination can make the top of the resist insoluble, blocking dissolution into the bulk of the resist (Figure 3-3). In extreme cases, no patterns can be observed after development. Another possible delay time acid loss mechanism is base contamination from the substrate, as has been observed on TiN substrates [3.17].

The effects of acid loss due to atmospheric base contaminants can be accounted for in a straightforward manner [3.18]. The base diffuses slowly from the top surface of the resist into the bulk. Assuming that the concentration of base contaminant in contact with the top of the resist remains constant, the diffusion equation can be solved for the concentration of base,  $B$ , as a function of depth into the resist film:

$$B = B_o \exp\left(-\left(z / \sigma\right)^2\right) \quad (3.39)$$



(a)



(b)

Figure 3-3. Atmospheric base contamination leads to T-top formation. Shown are line/space features printed in APEX-E for (a) 0.275 $\mu\text{m}$  features with no delay and (b) 0.325 $\mu\text{m}$  features with 10 minute delay between exposure and post-exposure bake (*courtesy of SEMATECH*).

where  $B_o$  is the base concentration at the top of the resist film,  $z$  is the depth into the resist ( $z=0$  at the top of the film) and  $\sigma$  is the diffusion length of the base in resist. The standard assumption of constant diffusivity has been made here so that diffusion length goes as the square root of the delay time.

Since the acid generated by exposure for most resist systems of interest is fairly strong, it is a good approximation to assume that all of the base contaminant will react with acid if there is sufficient acid present. Thus, the acid concentration at the beginning of the PEB,  $H^*$ , is related to the acid concentration after exposure,  $H$ , by

$$H^* = H - B \quad \text{or} \quad h^* = h - b \quad (3.40)$$

where the lower case symbols again represent the concentration relative to  $G_o$ , the initial photoacid generator concentration.

Acid loss during the PEB could occur by other mechanisms. For example, as the acid diffuses through the polymer, it may encounter sites which “trap” the acid, rendering it unusable for further amplification. If these traps were in much greater abundance than the acid itself (for example, sites on the polymer), the resulting acid loss rate would be first order,

$$\frac{\partial h}{\partial t'} = -K_{loss} h \quad (3.41)$$

where  $K_{loss}$  is the acid loss reaction rate constant. Of course, other more complicated acid loss mechanisms can be proposed, but in the absence of data supporting them, the simple first order loss mechanism is used here.

Acid can also be lost at the top surface of the resist due to evaporation. The amount of evaporation is a function of the size of the acid and the degree of its interaction with the resist polymer. A small acid (such as the trifluoroacetic acid discussed above) may have very significant evaporation. A separate rate equation can be written for the rate of evaporation of acid:

$$\left. \frac{\partial h}{\partial t'} \right|_{z=0} = -K_{evap} (h(0, t') - h_{air}(0, t')) \quad (3.42)$$

where  $z = 0$  is the top of the resist and  $h_{air}$  is the acid concentration in the atmosphere just above the photoresist surface. Typically, the PEB takes place in a reasonably open environment with enough air flow to eliminate any buildup of evaporated acid above the resist, making  $h_{air} = 0$ . If  $K_{evap}$  is very small, then virtually no evaporation takes place and we say that the top boundary of the resist is impenetrable. If  $K_{evap}$  is very large (resulting in evaporation that is much faster than the rate of diffusion), the effect is to bring the surface concentration of acid in the resist to zero. The significance of  $K_{evap}$  is best viewed by comparing the magnitude of  $K_{evap}$  to  $K_{amp}$  (i.e., how fast does evaporation occur relative to amplification).

The combination of a reacting system and a diffusing system is called a reaction-diffusion system. The solution of such a system is the simultaneous solution of equations (3.31) and (3.35) using equation (3.30) as an initial condition and equation (3.37) or (3.38) to describe the reaction-dependent diffusivity. Of course, any or all of the acid loss mechanisms can also be included. A convenient and straightforward method to solve such equations is the finite difference method (see, for example, reference [3.19]). The equations are solved by approximating the differential equations by difference equations. By marching through time and solving for all space at each time step, the final solution is the result after the final time step. A key part of an accurate solution is the choice of a sufficiently small time step. If the spatial dimension of interest is  $\Delta x$  (or  $\Delta y$  or  $\Delta z$ ), the time step should be chosen such that the diffusion length is less than  $\Delta x$  (using a diffusion length of about one third of  $\Delta x$  is common).

#### D. Measuring the ABC Parameters

Dill proposed a single, simple experiment for measuring the ABC parameters [3.4]. The photoresist to be measured is coated in a non-reflecting substrate (e.g., glass, quartz, or similar material). The resist is then exposed by a normally incident parallel beam of light at the wavelength of measurement. At the same time, the intensity of the light transmitted through the substrate is measured continuously. The output of the experiment, transmitted intensity as a function of exposure time, is then analyzed to determine the resist ABC parameters. A typical experimental setup is shown in Figure 3-4.

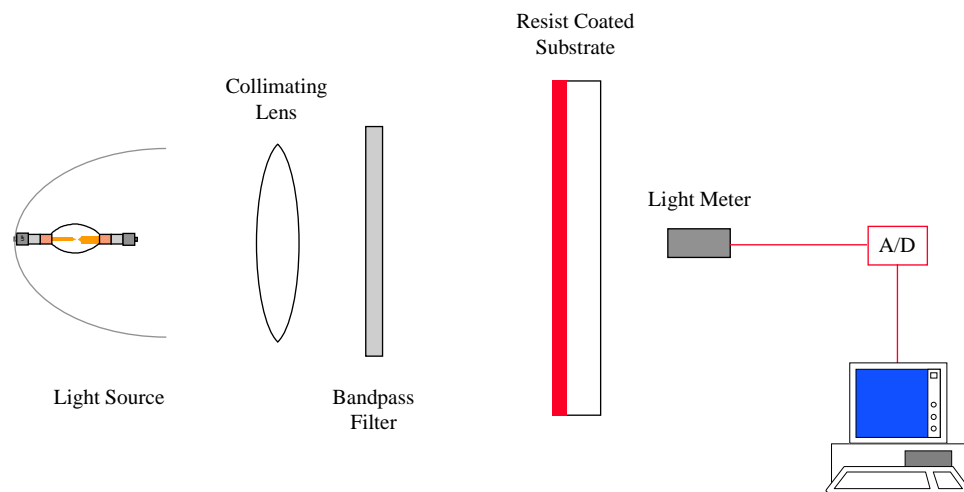


Figure 3-4. Experimental configuration for the measurement of the ABC parameters.

By measuring the incident exposing light intensity, the output of the experiment becomes overall transmittance as a function of incident exposure dose,  $T(E)$ . Figure 3-5 shows a typical result. Assuming careful measurement of this function, and a knowledge of the thickness of the photoresist, all that remains is the analysis of the data to extract the ABC parameters. Dill proposed two methods for extracting the parameters [3.4]. Those methods is reviewed here and a third, more accurate approach is shown.

Note that the effectiveness of this measurement technique rests with the non-zero value of  $A$ . If the photoresist does not change its optical properties with exposure (i.e., if  $A = 0$ ), then measuring transmittance will provide no insight on the exposure reaction, making  $C$  unobtainable by this method.

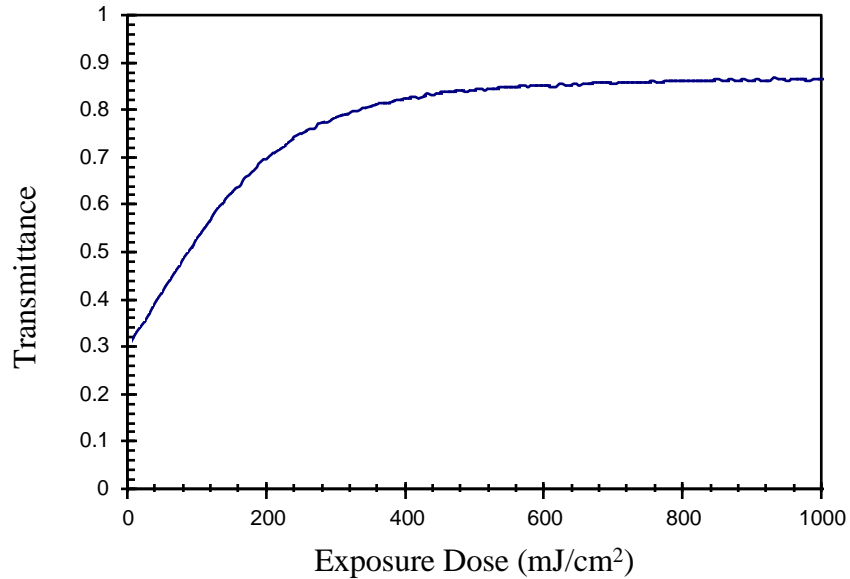


Figure 3-5. Typical transmittance curve of a positive  $g$ - or  $i$ -line bleaching photoresist measured using an apparatus similar to that pictured in Figure 3-4.

### 1. Graphical Data Analysis (Method 1)

Analysis of the experimental data is greatly simplified if the experimental conditions are adjusted so that the simple exposure and absorption equations (3.23) and (3.24) apply exactly. This means that light passing through the resist must not reflect at the resist/substrate interface. Further, light passing through the substrate must not reflect at the substrate/air interface. The first requirement is met by producing a transparent substrate with the same index of refraction as the photoresist. The second requirement is met by coating the backside of the substrate with an interference-type antireflection coating (ARC).

Given such ideal measurement conditions, Dill showed that the ABC parameters can be obtained from the transmittance curve by measuring the initial transmittance  $T(0)$ , the final (completely exposed) transmittance  $T(\infty)$ , and the initial slope of the curve. The relationships are:

$$A = \frac{1}{D} \ln \left( \frac{T(\infty)}{T(0)} \right) \quad (3.43a)$$

$$B = -\frac{1}{D}\ln(T(\infty)) \quad (3.43b)$$

$$C = \frac{A+B}{AT(0)\{1-T(0)\}T_{12}} \left. \frac{dT}{dE} \right|_{E=0} \quad (3.43c)$$

where  $D$  is the resist thickness and  $T_{12}$  is the transmittance of the air-resist interface and is given, for a resist index of refraction  $n_{resist}$ , by

$$T_{12} = 1 - \left( \frac{n_{resist} - 1}{n_{resist} + 1} \right)^2 \quad (3.44)$$

## 2. Differential Equation Solution (Method 2)

Although graphical analysis of the data is quite simple, it suffers from the common problem of errors when measuring the slope of experimental data. As a result, the value of  $C$  (and to a lesser extent,  $A$ ) obtained often contains significant error. Dill also proposed a second method for extracting the ABC parameters from the data. Again assuming that the ideal experimental conditions had been met, the ABC parameters could be obtained by directly solving the two coupled partial differential equations (3.23) and (3.24) and finding the values of  $A$ ,  $B$ , and  $C$  for which the solution best fits the experimental data. Obviously, fitting the entire experimental curve is much less sensitive to noise in the data than taking the slope at one point. Several techniques are available to provide a simple numerical solution [3.8-3.10].

## 3. Full Simulation (Method 3)

Methods 1 and 2 give accurate results only to the extent that the actual experimental conditions match the ideal (no reflection) conditions. In reality, there will always be some deviation from this ideal. Substrates will invariably have an index somewhat different that of the photoresist. And since the index of refraction of the photoresist changes with exposure, even a perfect substrate will be optically matched at only one instant in time during the experiment. Backside ARCs may also be less than perfect. In fact, most experimenters would prefer to use off-the-shelf glass or quartz wafers with no backside ARC. Under these conditions, how accurate are the extracted ABC parameters?

The dilemma can be solved by eliminating the restrictions of the ideal experiment. Rather than solving for the transmitted intensity via equations (3.23) and (3.24), one could use a lithography simulator to solve for the transmittance in a non-ideal case including changes in the resist index of refraction during exposure and reflections from both the top and bottom of the substrate. Then, by adjusting the ABC parameters, a best fit of the model to the data could be obtained. This method provides the ultimate accuracy in obtaining extracted ABC parameters [3.20].

## References

- 3.1 D. A. Skoog and D. M. West, Fundamentals of Analytical Chemistry, 3rd edition, Holt, Rinehart, and Winston (New York :1976), pp. 509-510.
- 3.2 J. M. Koyler, et al., "Thermal Properties of Positive Photoresist and their Relationship to VLSI Processing," *Kodak Microelectronics Seminar Interface '79*, (1979) pp. 150-165.
- 3.3 J. M. Shaw, M. A. Frisch, and F. H. Dill, "Thermal Analysis of Positive Photoresist Films by Mass Spectrometry," *IBM Jour. Res. Dev.*, Vol 21 (May, 1977), pp. 219-226.
- 3.4 F. H. Dill, W. P. Hornberger, P. S. Hauge, and J. M. Shaw, "Characterization of Positive Photoresist," *IEEE Trans. Electron Devices*, Vol. ED-22, No. 7, (July, 1975) pp. 445-452.
- 3.5 C. A. Mack, "Absorption and Exposure in Positive Photoresist," *Applied Optics*, Vol. 27, No. 23 (1 Dec. 1988) pp. 4913-4919.
- 3.6 R. Dammel, Diazonaphthoquinone-based Resists, SPIE Tutorial Texts Vol. TT 11 (Bellingham, WA: 1993).
- 3.7 J. Albers and D. B. Novotny, "Intensity Dependence of Photochemical Reaction Rates for Photoresists," *Jour. Electrochem. Soc.*, Vol. 127, No. 6 (June, 1980) pp. 1400-1403.
- 3.8 C. E. Herrick, Jr., "Solution of the Partial Differential Equations Describing Photo-decomposition in a Light-absorbing Matrix having Light-absorbing Photoproducts," *IBM Journal of Research and Development*, Vol. 10 (Jan., 1966) pp. 2-5.
- 3.9 J. J. Diamond and J. R. Sheats, "Simple Algebraic Description of Photoresist Exposure and Contrast Enhancement," *IEEE Electron Device Letters*, Vol. EDL-7, No. 6 (June, 1986) pp. 383-386.
- 3.10 S. V. Babu and E. Barouch, "Exact Solution of Dill's Model Equations for Positive Photoresist Kinetics," *IEEE Electron Device Letters*, Vol. EDL-7, No. 4 (April, 1986) pp. 252-253.
- 3.11 H. Ito and C. G. Willson, "Applications of Photoinitiators to the Design of Resists for Semiconductor Manufacturing," in Polymers in Electronics, ACS Symposium Series 242 (1984) pp. 11-23.
- 3.12 D. Seligson, S. Das, H. Gaw, and P. Pianetta, "Process Control with Chemical Amplification Resists Using Deep Ultraviolet and X-ray Radiation," *Jour. Vacuum Science and Tech.*, Vol. B6, No. 6 (Nov/Dec, 1988) pp. 2303-2307.
- 3.13 C. A. Mack, D. P. DeWitt, B. K. Tsai, and G. Yetter, "Modeling of Solvent Evaporation Effects for Hot Plate Baking of Photoresist," *Advances in Resist Technology and Processing XI, Proc.*, SPIE Vol. 2195 (1994) pp. 584-595.
- 3.14 H. Fujita, A. Kishimoto, and K. Matsumoto, "Concentration and Temperature Dependence of Diffusion Coefficients for Systems Polymethyl Acrylate and n-Alkyl Acetates," *Transactions of the Faraday Society*, Vol. 56 (1960) pp. 424-437.
- 3.15 D. E. Bornside, C. W. Macosko and L. E. Scriven, "Spin Coating of a PMMA/Chlorobenzene Solution," *Journal of the Electrochemical Society*, Vol. 138, No. 1 (Jan., 1991) pp. 317-320.
- 3.16 S. A. MacDonald, et al., "Airborne Chemical Contamination of a Chemically Amplified Resist," *Advances in Resist Technology and Processing VIII, Proc.*, SPIE Vol. 1466 (1991) pp. 2-12.
- 3.17 K. R. Dean and R. A. Carpio, "Contamination of Positive Deep-UV Photoresists," *OCG Microlithography Seminar Interface '94, Proc.*, (1994) pp. 199-212.
- 3.18 T. Ohfuji, A. G. Timko, O. Nalamasu, and D. R. Stone, "Dissolution Rate Modeling of a Chemically Amplified Positive Resist," *Advances in Resist Technology and Processing X, Proc.*, SPIE Vol. 1925 (1993) pp. 213-226.
- 3.19 F. P. Incropera and D. P. DeWitt, Fundamentals of Heat and Mass Transfer, 3rd edition, John Wiley & Sons (New York: 1990).

- 3.20 C. A. Mack, T. Matsuzawa, A. Sekiguchi, Y. Minami, “Resist Metrology for Lithography Simulation, Part 1: Exposure Parameter Measurements,” *Metrology, Inspection, and Process Control for Microlithography X, Proc.*, SPIE Vol. 2725 (1996) pp. 34-48.

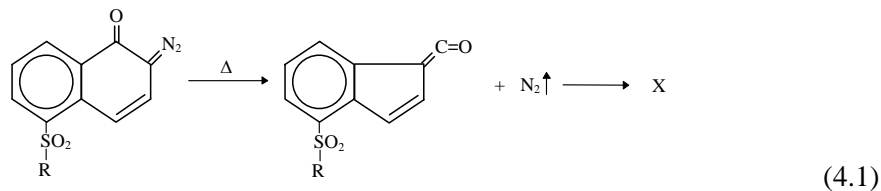
# Chapter 4

## Photoresist Bake Effects

Baking a resist may have many purposes, from removing solvent to causing chemical amplification. In addition to the intended results, baking may also cause numerous unintended outcomes. For example, the light sensitive component of the resist may decompose at temperatures typically used to remove solvent. Baking a photoresist remains one of the most complicated and least understood steps in the lithographic process. In this chapter, the impact of baking on thermal decomposition and diffusion of the photoactive material is considered. The impact of baking on solvent diffusion is discussed in Chapters 6 and 7.

### A. Prebake Thermal Decomposition

The purpose of a photoresist prebake (also called post apply bake) is to dry the resist after spin coating by removing solvent from the film. However, as with most thermal processing steps, the bake has other effects on the photoresist. When heated to temperatures above about 70°C, the photoactive compound (PAC) of a diazo-type positive photoresist begins to decompose to a non-photosensitive product. The initial reaction mechanism is thought to be identical to that of the PAC reaction during ultraviolet exposure [4.1-4.4].



The identity of the product  $X$  is discussed below.

To determine the concentration of PAC as a function of prebake time and temperature, consider the first order decomposition reaction,



where  $M$  is the photoactive compound. If we let  $M'_o$  be the concentration of PAC before prebake and  $M_o$  the concentration of PAC after prebake, simple kinetics tells us that

$$\begin{aligned}\frac{dM_o}{dt} &= -K_T M_o \\ M_o &= M'_o \exp(-K_T t_b) \\ m' &= \exp(-K_T t_b)\end{aligned}\quad (4.3)$$

where  $t_b$  = bake time,  
 $K_T$  = decomposition rate constant at absolute temperature  $T$ , and  
 $m' = M_o/M'_o$ , the fraction of PAC remaining after the bake.

The dependence of  $K_T$  upon temperature may be described by the Arrhenius equation,

$$K_T = A_r \exp(-E_a / RT) \quad (4.4)$$

where  $A_r$  = Arrhenius coefficient,  
 $E_a$  = activation energy, and  
 $R$  = universal gas constant.

Thus, the two parameters  $E_a$  and  $A_r$  allow us to know  $m'$  as a function of the prebake conditions, provided Arrhenius behavior is followed. In polymer systems, caution must be exercised since bake temperatures near the glass transition temperature sometimes leads to non-Arrhenius behavior. For normal prebakes of typical photoresists, the Arrhenius model appears well founded.

The effect of this decomposition is a change in the chemical makeup of the photoresist. Thus, any parameters which are dependent upon the quantitative composition of the resist are also dependent upon prebake. The most important of these parameters fall into three categories: 1) optical (exposure) parameters such as the resist absorption coefficient, 2) diffusion parameters during post-exposure bake, and 3) development parameters such as the development rates of unexposed and completely exposed resist. A technique is described to measure  $E_a$  and  $A_r$  and thus begin to quantify these effects of prebake.

In the model proposed by Dill et al. [4.5], the exposure of a positive photoresist can be characterized by the three parameters  $A$ ,  $B$ , and  $C$ .  $A$  and  $B$  are related to the optical absorption coefficient of the photoresist,  $\alpha$ , and  $C$  is the overall rate constant of the exposure reaction. More specifically,

$$\begin{aligned}\alpha &= Am + B \\ A &= (a_M - a_P)M_o \\ B &= a_P M_o + a_R R + a_S S\end{aligned}\quad (4.5)$$

where  $a_M$  = molar absorption coefficient of the photoactive compound  $M$ ,  
 $a_P$  = molar absorption coefficient of the exposure product  $P$ ,  
 $a_S$  = molar absorption coefficient of the solvent  $S$ ,  
 $a_R$  = molar absorption coefficient of the resin  $R$ ,  
 $M_o$  = the PAC concentration at the start of the exposure (i.e., after prebake), and  
 $m = M/M_o$ , the relative PAC concentration as a result of exposure.

These expressions do not explicitly take into account the effects of prebake on the resist composition. To do so, we can modify equation (4.5) to include absorption by the component  $X$ .

$$B = a_P M_o + a_R R + a_X X \quad (4.6)$$

where  $a_X$  is the molar absorption coefficient of the decomposition product  $X$  (and the absorption term for the solvent has been neglected for simplicity). The stoichiometry of the decomposition reaction gives

$$X = M'_o - M_o \quad (4.7)$$

Thus,

$$B = a_P M_o + a_R R + a_X (M'_o - M_o) \quad (4.8)$$

Let us consider two cases of interest, no bake (NB) and full bake (FB). When there is no prebake (meaning no decomposition),  $M_o = M'_o$  and

$$\begin{aligned} A_{NB} &= (a_M - a_P) M'_o \\ B_{NB} &= a_P M'_o + a_R R \end{aligned} \quad (4.9)$$

We shall define full bake as a prebake which decomposes all PAC. Thus  $M_o = 0$  and

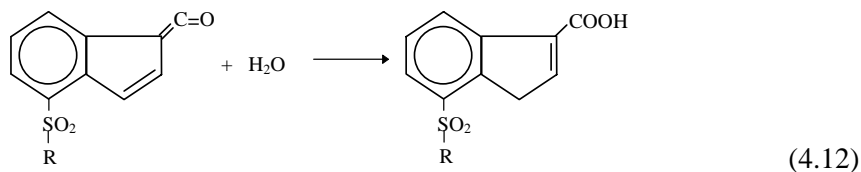
$$\begin{aligned} A_{FB} &= 0 \\ B_{FB} &= a_X M'_o + a_R R \end{aligned} \quad (4.10)$$

Using these special cases in our general expressions for  $A$  and  $B$ , we can show explicitly how these two parameters vary with PAC decomposition:

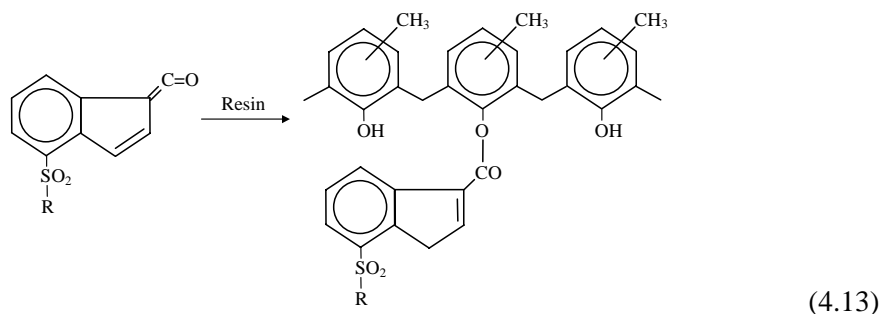
$$\begin{aligned} A &= A_{NB} m' \\ B &= B_{FB} - (B_{FB} - B_{NB}) m' \end{aligned} \quad (4.11)$$

The  $A$  parameter decreases linearly as decomposition occurs, and  $B$  typically increases slightly.

The development rate is, of course, dependent on the concentration of PAC in the photoresist. However, the product  $X$  can also have a large effect on the development rate. Several studies have been performed to determine the composition of the product  $X$  [4.2-4.4]. The results indicate that there are two possible products and the most common outcome of a prebake decomposition is a mixture of the two. The first product is formed via the reaction (4.12) and is identical to the product of UV exposure.



As can be seen, this reaction requires the presence of water. A second reaction, which does not require water, is the esterification of the ketene with the resin.



Both possible products have a dramatic effect on dissolution rate. The carboxylic acid is very soluble in developer and enhances dissolution. The formation of carboxylic acid can be thought of as a blanket exposure of the resist. The dissolution rate of unexposed resist ( $r_{min}$ ) will increase due to the presence of the carboxylic acid. The dissolution rate of fully exposed resist ( $r_{max}$ ), however, will not be affected. Since the chemistry of the dissolution process is unchanged, the basic shape of the development rate function will also remain unchanged.

The ester, on the other hand, is very difficult to dissolve in aqueous solutions and thus retards the dissolution process. It will have the effect of decreasing  $r_{max}$ , although the effects of ester formation on the full dissolution behavior of a resist are not well known.

If the two mechanisms given in equations (4.12) and (4.13) are taken into account, the rate equation (4.3) will become

$$\frac{dM_o}{dt} = -k_1 M_o - k_2 [\text{H}_2\text{O}] M_o$$

(4.14)

where  $k_1$  and  $k_2$  are the rate constants of equations (4.12) and (4.13), respectively. For a given concentration of water in the resist film this reverts to equation (4.3) where

$$K_T = k_1 + k_2 [\text{H}_2\text{O}]$$

(4.15)

Thus, the relative importance of the two reactions will depend not only on the ratio of the rate constants but on the amount of water in the resist film. The concentration of water is a function of atmospheric conditions during the bake and the past history of the resist coated wafer. Further experimental measurements of development rate as a function of prebake temperature are needed to quantify these effects.

Examining equation (4.11), one can see that the parameter  $A$  can be used as a means of measuring  $m'$ , the fraction of PAC remaining after prebake. Thus, by measuring  $A$  as a function of prebake time and temperature, one can determine the activation energy and the corresponding Arrhenius coefficient for the proposed decomposition reaction. Using the technique given by Dill et al. [4.5] and described in the previous chapter,  $A$ ,  $B$  and  $C$  can be easily determined by measuring the optical transmittance of a thin photoresist film on a glass substrate while the resist is being exposed.

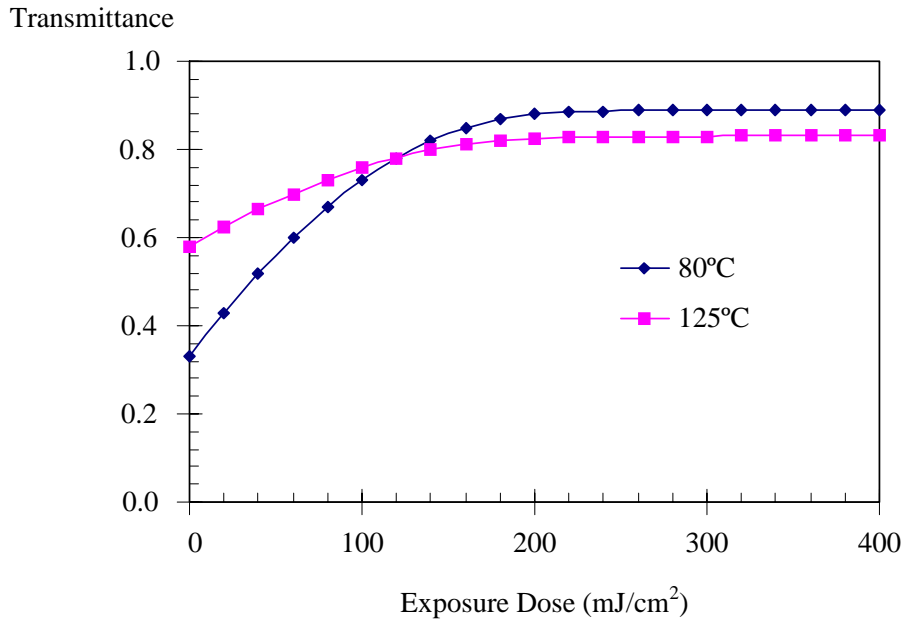


Figure 4-1. Two transmittance curves for Kodak 820 resist at 365nm. The curves are for a convection oven prebake of 30 minutes at the temperatures shown [4.6].

Examples of measured transmittance curves are given in Figure 4-1, where transmittance is plotted versus exposure dose. The different curves represent different prebake temperatures. For every curve,  $A$ ,  $B$ , and  $C$  can be calculated. Figure 4-2 shows the variation of the resist parameter  $A$  with prebake conditions. According to equations (4.3) and (4.11), this variation should take the form

$$\frac{A}{A_{NB}} = e^{-K_r t_b}$$

$$\ln\left(\frac{A}{A_{NB}}\right) = -K_T t_b \quad (4.17)$$

Thus, a plot of  $\ln(A)$  versus bake time should give a straight line with a slope equal to  $-K_T$ . This plot is shown in Figure 4-3. Knowing  $K_T$  as a function of temperature, one can determine the activation energy and Arrhenius coefficient from equation (4.4). One should note that the parameters  $A_{NB}$ ,  $B_{NB}$  and  $B_{FB}$  are wavelength dependent, but  $E_a$  and  $A_r$  are not.

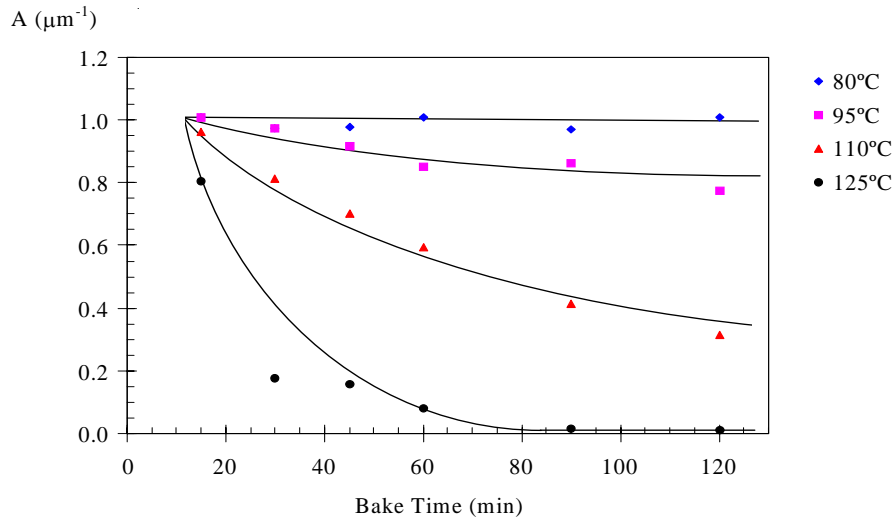


Figure 4-2. The variation of the resist absorption parameter  $A$  with prebake time and temperature for Kodak 820 resist at 365nm [4.6].

Figure 4-2 shows an anomaly in which there is a lag time before decomposition occurs. This lag time is the time it took the wafer and wafer carrier to reach the temperature of the convection oven. Equation (4.3) can be modified to accommodate this phenomena,

$$m' = e^{-K_T(t_b - t_{wup})} \quad (4.18)$$

where  $t_{wup}$  is the warm up time. A lag time of about 11 minutes was observed when convection oven baking a 1/4" thick glass substrate in a wafer carrier. When a 60 mil glass wafer was used without a carrier, the warm-up time was under 5 minutes and could not be measured accurately in this experiment [4.6].

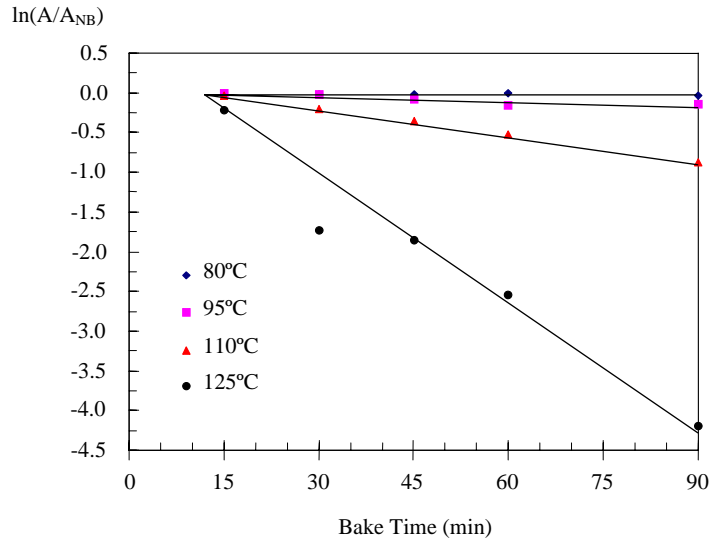


Figure 4-3. Log plot of the resist absorption parameter  $A$  with prebake time and temperature for Kodak 820 resist at 365 nm [4.6].

Although all the data presented thus far has been for convection oven prebake, the above method of evaluating the effects of prebake can also be applied to hot-plate prebaking. For the data presented in Figure 4-3, the activation energy is 30.3 Kcal/mol and the natural logarithm of the Arrhenius coefficient (in 1/minutes) is 35.3 [4.6]. Thus, a 100°C, 30 minute convection oven prebake would decompose 11% of the photoactive compound.

## B. Post-Exposure Bake

Many attempts have been made to reduce the standing wave effect and thus increase linewidth control and resolution. One particularly useful method is the post-exposure, pre-development bake as described by Walker [4.7]. A 100°C oven bake for 10 minutes was found to reduce the standing wave ridges on a resist sidewall significantly. This phenomenon can be explained quite simply as the diffusion of photoactive compound (PAC) in the resist during the high temperature bake. A mathematical model which predicts the results of such a post-exposure bake (PEB) is described below.

In general, molecular diffusion is governed by Fick's Second Law of Diffusion, which states (in one dimension)

$$\frac{\partial C_A}{\partial t} = D \frac{\partial^2 C_A}{\partial t^2} \quad (4.19)$$

where  $C_A$  = concentration of species A  
 $D$  = diffusion coefficient of A at some temperature  $T$   
 $t$  = time that the system is at temperature  $T$ .

Note that the diffusion coefficient is assumed to be independent of concentration here. This differential equation can be solved given a set of boundary conditions and an initial distribution of A. One possible initial condition is known as the impulse source. At some point  $x_o$  there are  $N$  moles of substance A and at all other points there is no A. Thus, the concentration at  $x_o$  is infinite. Given this initial distribution of A, the solution to equation (4.19) is the Gaussian distribution function,

$$C_A(x) = \frac{N}{\sqrt{2\pi\sigma^2}} e^{-r^2/2\sigma^2} \quad (4.20)$$

where  $\sigma = \sqrt{2Dt}$ , the diffusion length, and  $r = x - x_o$ .

In practice there are no impulse sources. Instead, we can approximate an impulse source as having some concentration  $C_o$  over some small distance  $\Delta x$  centered at  $x_o$ , with zero concentration outside of this range. An approximate form of equation (4.20) is then

$$C_A(x) \cong \frac{C_o \Delta x}{\sqrt{2\pi\sigma^2}} e^{-r^2/2\sigma^2} \quad (4.21)$$

This solution is fairly accurate if  $\Delta x < 3\sigma$ . If there are two “impulse” sources located at  $x_1$  and  $x_2$ , with initial concentrations  $C_1$  and  $C_2$  each over a range  $\Delta x$ , the concentration of A at  $x$  after diffusion is

$$C_A(x) = \left[ \frac{C_1}{\sqrt{2\pi\sigma^2}} e^{-r_1^2/2\sigma^2} + \frac{C_2}{\sqrt{2\pi\sigma^2}} e^{-r_2^2/2\sigma^2} \right] \Delta x \quad (4.22)$$

where  $r_1 = x - x_1$  and  $r_2 = x - x_2$ .

If there are a number of sources equation (4.22) becomes

$$C_A(x) = \frac{\Delta x}{\sqrt{2\pi\sigma^2}} \sum_n C_n e^{-r_n^2/2\sigma^2} \quad (4.23)$$

Extending the analysis to a continuous initial distribution  $C_o(x)$ , equation (4.23) becomes

$$C_A(x) = \frac{1}{\sqrt{2\pi\sigma^2}} \int_{-\infty}^{\infty} C_o(x - x') e^{-x'^2/2\sigma^2} dx' \quad (4.24)$$

where  $x'$  is now the distance from the point  $x$ . Equation (4.24) is simply the convolution of two functions.

$$C_A(x) = C_o(x) * f(x) \quad (4.25)$$

where

$$f(x) = \frac{1}{\sqrt{2\pi\sigma^2}} e^{-x^2/2\sigma^2}$$

This equation can now be made to accommodate two dimensional diffusion.

$$C_A(x, y) = C_o(x, y) * f(x, y) \quad (4.26)$$

where

$$f(x, y) = \frac{1}{2\pi\sigma^2} e^{-r^2/2\sigma^2}$$

$$r = \sqrt{x^2 + y^2}$$

Three-dimensional diffusion can similarly be calculated.

We are now ready to apply equation (4.26) to the diffusion of PAC in a photoresist during a post-exposure bake. For a two-dimensional case, the PAC distribution after exposure can be described by  $m(x, z)$ , where  $m$  is the relative PAC concentration. According to equation (4.26) the relative PAC concentration after a post-exposure bake,  $m^*(x, z)$ , is given by

$$m^*(x, z) = \frac{1}{2\pi\sigma^2} \int_{-\infty}^{\infty} \int_{-\infty}^{\infty} m(x-x', z-z') e^{-r'^2/2\sigma^2} dx' dz' \quad (4.27)$$

In evaluating equation (4.27) it is common to replace the integrals by summations over intervals  $\Delta x$  and  $\Delta z$ . In such a case, the restrictions that  $\Delta x < 3\sigma$  and  $\Delta z < 3\sigma$  will apply. An alternative solution is to solve the diffusion equation (4.19) directly, for example using a finite difference approach. The boundary conditions typically assume the wafer and air interfaces are impenetrable.

The diffusion model can now be used to simulate the effects of a post-exposure bake. Using a full lithography simulation package, a simulated resist profile can be generated. By including the model for a post-exposure bake, the profile can be generated showing how the standing wave effect is reduced (Figure 4-4). The only parameter that needs to be specified in equation (4.27) is the diffusion length  $\sigma$ , or equivalently, the diffusion coefficient  $D$  and the bake time  $t$ . In turn,  $D$  is a function of the bake temperature  $T$  and, of course, the resist system used. Thus, if the functionality of  $D$  with temperature is known for a given resist system, a PEB of time  $t$  and temperature  $T$  can be modeled. A general temperature dependence for the diffusivity  $D$  can be found using the Arrhenius equation (for temperature ranges which do not traverse the glass transition temperature).

$$D = D_o e^{-E_a/RT} \quad (4.28)$$

where  $D_o$  = Arrhenius constant (units of  $\text{nm}^2/\text{s}$ ),

$E_a$  = activation energy,

$R$  = universal gas constant, and

$T$  = temperature in Kelvin.

Unfortunately, very little work has been done in measuring the diffusivity of photoactive compounds in photoresist. From Walker's work [4.7], one can estimate the values of  $E_a$  and  $D_o$  to be about 35 Kcal/mol and  $3.2 \times 10^{21} \text{ nm}^2/\text{s}$ , respectively.

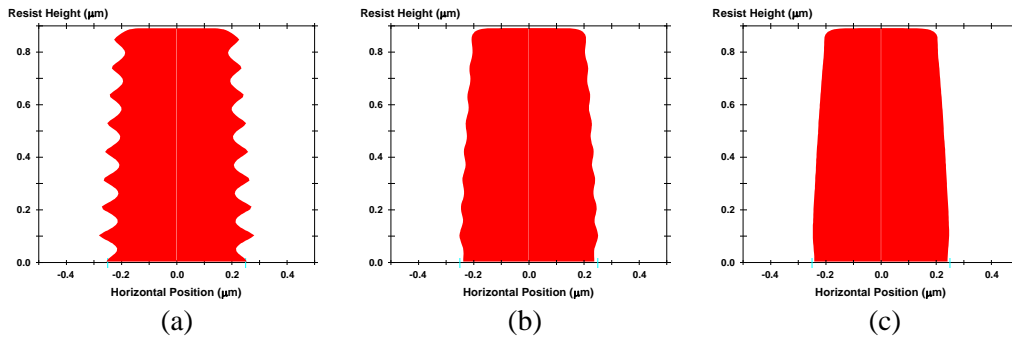


Figure 4-4. Photoresist profile simulations as a function of the PEB diffusion length: (a) 20nm, (b) 40nm, and (c) 60nm.

## References

- 4.1 F. H. Dill and J. M. Shaw, "Thermal Effects on the Photoresist AZ1350J," *IBM Jour. Res. Dev.*, Vol. 21, No. 3, (May, 1977) pp. 210-218.
- 4.2 J. M. Shaw, M. A. Frisch and F. H. Dill, "Thermal Analysis of Positive Photoresist Films by Mass Spectrometry," *IBM Jour. Res. Dev.*, Vol. 21, No. 3, (May, 1977) pp. 219-226.
- 4.3 J. M. Koyler, F. Z. Custode and R. L. Ruddell, "Thermal Properties of Positive Photoresist and their relationship to VLSI Processing," *Kodak Interface '79*, (Nov. 1979) pp. 150-165.
- 4.4 D. W. Johnson, "Thermolysis of Positive Photoresists," *Adv. Resist Tech., Proc.*, SPIE Vol. 469, (1984) pp. 72-79.
- 4.5 F. H. Dill, et al., "Characterization of Positive Photoresists," *IEEE Trans. Electron Devices*, Vol. ED-22, No. 7, (July, 1975) pp. 445-452.
- 4.6 C. A. Mack and R. T. Carback, "Modeling the Effects of Prebake on Positive Resist Processing," *Kodak Microelectronics Seminar, Proc.*, (1985) pp. 155-158.
- 4.7 E. J. Walker, "Reduction of Photoresist Standing-Wave Effects by Post-Exposure Bake," *IEEE Trans. Electron Devices.*, Vol. ED- 22, No. 7 (July, 1975) pp. 464-466.

# Chapter 5

## Photoresist Development

An overall resist processing model requires a mathematical representation of the development process. Many previous attempts have taken the form of empirical fits to development rate data as a function of exposure [5.1,5.2]. The models formulated below begin on a more fundamental level, with a postulated reaction mechanism which then leads to a development rate equation [5.3,5.4]. The rate constants involved can be determined by comparison with experimental data. Deviations from the expected development rates have been reported under certain conditions at the surface of the resist. This effect, called surface induction or surface inhibition, can be related empirically to the expected development rate, i.e., to the bulk development rate as predicted by a kinetic model.

Unfortunately, fundamental experimental evidence of the exact mechanism of photoresist development is lacking. The models presented below are reasonable, and the resulting rate equations have been shown to describe actual development rates extremely well. However, faith in the exact details of the mechanism is limited by this dearth of fundamental studies.

### A. Kinetic Development Model

In order to derive an analytical development rate expression, a kinetic model of the development process will be used. This approach involves proposing a reasonable mechanism for the development reaction and then applying standard kinetics to this mechanism in order to derive a rate equation. We shall assume that the development of a diazo-type positive photoresist involves three processes: diffusion of developer from the bulk solution to the surface of the resist, reaction of the developer with the resist, and diffusion of the product back into the solution. For this analysis, we shall assume that the last step, diffusion of the dissolved resist into solution, occurs very quickly so that this step may be ignored. Let us now look at the first two steps in the proposed mechanism. The diffusion of developer to the resist surface can be described with the simple diffusion rate equation, given approximately by

$$r_D = k_D(D - D_S) \quad (5.1)$$

where  $r_D$  is the rate of diffusion of the developer to the resist surface,  $D$  is the bulk developer concentration,  $D_S$  is the developer concentration at the resist surface, and  $k_D$  is the rate constant.

We shall now propose a mechanism for the reaction of developer with the resist. The resist is composed of large macromolecules of resin  $R$  along with a photoactive compound  $M$ , which converts to product  $P$  upon exposure to UV light. The resin is somewhat soluble in the developer solution, but the presence of the PAC (photoactive compound) acts as an inhibitor to dissolution, making the development rate very slow. The product  $P$ , however, is very soluble in developer, enhancing the dissolution rate of the resin. Let us assume that  $n$  molecules of product  $P$  react with the developer to dissolve a resin molecule. The rate of the reaction is

$$r_R = k_R D_S P^n \quad (5.2)$$

where  $r_R$  is the rate of reaction of the developer with the resist and  $k_R$  is the rate constant. (Note that the mechanism shown in equation (5.2) is the same as the “polyphotolysis” model described by Trefonas and Daniels [5.5].) From the stoichiometry of the exposure reaction,

$$P = M_o - M \quad (5.3)$$

where  $M_o$  is the initial PAC concentration (i.e., before exposure).

The two steps outlined above are in series, i.e., one reaction follows the other. Thus, the two steps will come to a steady state such that

$$r_R = r_D = r \quad (5.4)$$

Equating the rate equations, one can solve for  $D_S$  and eliminate it from the overall rate equation, giving

$$r = \frac{k_D k_R D P^n}{k_D + k_R P^n} \quad (5.5)$$

Using equation (5.3) and letting  $m = M/M_o$ , the relative PAC concentration, equation (5.5) becomes

$$r = \frac{k_D D (1 - m)^n}{k_D / k_R M_o^n + (1 - m)^n} \quad (5.6)$$

When  $m = 1$  (resist unexposed), the rate is zero. When  $m = 0$  (resist completely exposed), the rate is equal to  $r_{max}$  where

$$r_{max} = \frac{k_D D}{k_D / k_R M_o^n + 1} \quad (5.7)$$

If we define a constant  $a$  such that

$$a = k_D / k_R M_o^n \quad (5.8)$$

the rate equation becomes

$$r = r_{\max} \frac{(a+1)(1-m)^n}{a+(1-m)^n} \quad (5.9)$$

Note that the simplifying constant  $a$  describes the rate constant of diffusion relative to the surface reaction rate constant. A large value of  $a$  will mean that diffusion is very fast, and thus less important, compared to the fastest surface reaction (for completely exposed resist).

There are three constants that must be determined experimentally,  $a$ ,  $n$ , and  $r_{\max}$ . The constant  $a$  can be put in a more physically meaningful form as follows. A characteristic of some experimental rate data is an inflection point in the rate curve at about  $m = 0.2-0.7$ . The point of inflection can be calculated by letting

$$\frac{d^2r}{dm^2} = 0$$

giving

$$a = \frac{(n+1)}{(n-1)}(1-m_{TH})^n \quad (5.10)$$

where  $m_{TH}$  is the value of  $m$  at the inflection point, called the threshold PAC concentration.

This model does not take into account the finite dissolution rate of unexposed resist ( $r_{\min}$ ). One approach is simply to add this term to equation (5.9), giving

$$r = r_{\max} \frac{(a+1)(1-m)^n}{a+(1-m)^n} + r_{\min} \quad (5.11)$$

This approach assumes that the mechanism of development of the unexposed resist is independent of the above-proposed development mechanism. In other words, there is a finite dissolution of resist that occurs by a mechanism that is independent of the presence of exposed PAC. Note that the addition of the  $r_{\min}$  term means that the true maximum development rate is actually  $r_{\max} + r_{\min}$ . In most cases  $r_{\max} \gg r_{\min}$  and the difference is negligible.

Consider the case when the diffusion rate constant is large compared to the surface reaction rate constant. If  $a \gg 1$ , the development rate equation (5.11) will become

$$r = r_{\max} (1-m)^n + r_{\min} \quad (5.12)$$

The interpretation of  $a$  as a function of the threshold PAC concentration  $m_{TH}$  given by equation (5.10) means that a very large  $a$  would correspond to a large negative value of  $m_{TH}$ . In other words, if the surface reaction is very slow compared to the mass transport of developer to the surface there will be no inflection point in the development rate data and equation (5.12) will apply. It is quite apparent that equation (5.12) could be derived directly from equation (5.2) if the diffusion step were ignored.

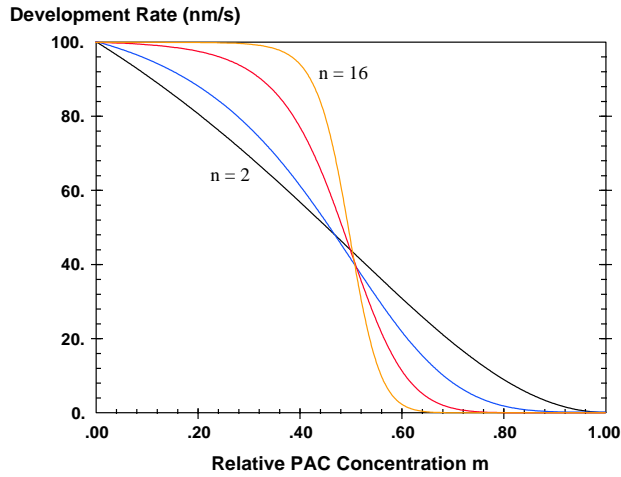


Figure 5-1. Development rate plot of the Original Mack model as a function of the dissolution selectivity parameter ( $r_{max} = 100$  nm/s,  $r_{min} = 0.1$  nm/s,  $m_{TH} = 0.5$ , and  $n = 2, 4, 8, \text{ and } 16$ ).

Figure 5-1 shows some plots of the model of equation (5.11) for different values of  $n$ . The behavior of the dissolution rate with increasing  $n$  values is to make the rate function more “selective” between resist exposed above  $m_{TH}$  and resist exposed below  $m_{TH}$ . For this reason,  $n$  is called the dissolution selectivity parameter. Also from this behavior, the interpretation of  $m_{TH}$  as a “threshold” concentration becomes quite evident.

## B. Enhanced Kinetic Development Model

The previous kinetic model is based on the principle of dissolution enhancement. The carboxylic acid enhances the dissolution rate of the resin/PAC mixture. In reality this is a simplification -- there are really two mechanisms at work. The PAC acts to inhibit dissolution of the resin while the acid acts to enhance dissolution. Thus, a development rate expression could reflect both of these mechanisms. A new model, call the enhanced kinetic model, was proposed to include both effects [5.4]:

$$r = r_{resin} \frac{1 + k_{enh}(1 - m)^n}{1 + k_{inh}(m)^l} \quad (5.13)$$

where  $k_{enh}$  is the rate constant for the enhancement mechanism,  $n$  is the enhancement reaction order,  $k_{inh}$  is the rate constant for the inhibition mechanism,  $l$  is the inhibition reaction order, and  $r_{resin}$  is the development rate of the resin alone.

For no exposure,  $m = 1$  and the development rate is at its minimum. From equation (5.13),

$$r_{min} = \frac{r_{resin}}{1 + k_{inh}} \quad (5.14)$$

Similarly, when  $m = 0$ , corresponding to complete exposure, the development is at its maximum.

$$r_{max} = r_{resin} (I + k_{enh}) \quad (5.15)$$

Thus, the development rate expression can be characterized by five parameters:  $r_{max}$ ,  $r_{min}$ ,  $r_{resin}$ ,  $n$ , and  $l$ .

Obviously, the enhanced kinetic model for resist dissolution is a superset of the original kinetic model. If the inhibition mechanism is not important, then  $k_{inh} = 0$ . For this case, equation (5.13) is identical to equation (5.12) when

$$r_{min} = r_{resin}, \quad r_{max} = r_{resin} k_{enh} \quad (5.16)$$

The enhanced kinetic model of equation (5.13) assumes that mass transport of developer to the resist surface is not significant. Of course, a simple diffusion of developer can be added to this mechanism as was done above with the original kinetic model. Figure 5-2 shows several plots of the model of equation (5.13).

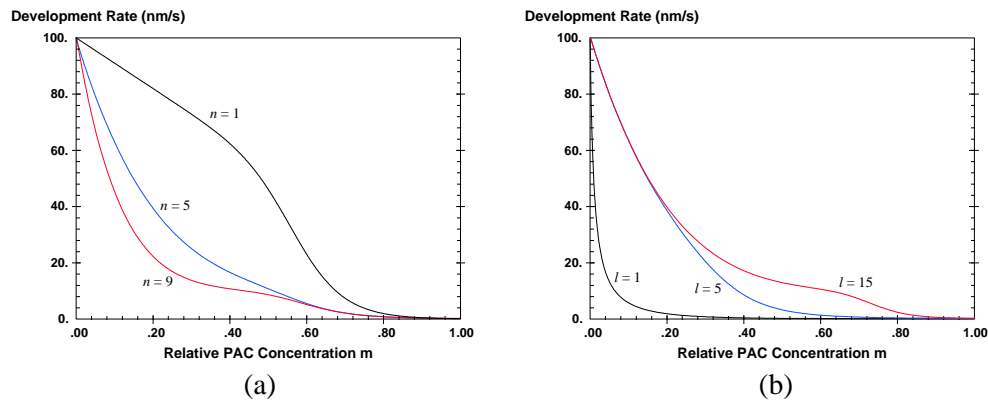


Figure 5-2. Plots of the Enhanced Mack development model for  $r_{max} = 100$  nm/s,  $r_{resin} = 10$  nm/s,  $r_{min} = 0.1$  nm/s and (a)  $l = 9$ , and (b)  $n = 5$ .

### C. Surface Inhibition

The kinetic models given above predict the development rate of the resist as a function of the photoactive compound concentration remaining after the resist has been exposed to UV light. There are, however, other parameters that are known to affect the development rate, but which were not included in this model. The most notable deviation from the kinetic theory is the surface inhibition effect. The inhibition, or surface induction, effect is a decrease in the expected development rate at the surface of the resist [5.6-5.8]. Thus, this effect is a function of the depth into the resist and requires a new description of development rate.

Several factors have been found to contribute to the surface inhibition effect. Baking of the photoresist can produce surface inhibition and two possible mechanisms are thought to be likely causes. One possibility is an oxidation of the resist at the resist surface, resulting in reduced development rate of the oxidized film [5.6-5.8]. Alternatively, the induction effect may be the result of reduced solvent

content near the resist surface, which also results from baking the resist [5.9]. Both mechanisms could be contributing to the surface inhibition. Finally, surface inhibition can be induced with the use of surfactants in the developer.

An empirical model can be used to describe the positional dependence of the development rate. If we assume that the development rate near the surface of the resist exponentially approaches the bulk development rate, the rate as a function of depth,  $r(z)$ , is

$$r(z) = r_B \left( 1 - (1 - r_o) e^{-z/\delta} \right) \quad (5.17)$$

where  $r_B$  is the bulk development rate as given by equation (5.11) or (5.13),  $r_o$  is the development rate at the surface of the resist relative to  $r_B$ , and  $\delta$  is the depth of the surface inhibition layer. In several resists, the induction effect has been found to take place over a depth of about 100 nm [5.6,5.8].

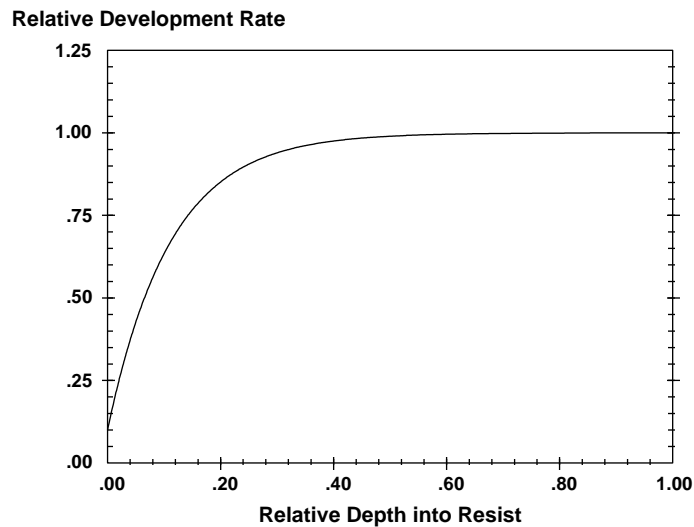


Figure 5-3. Example surface inhibition with  $r_o = 0.1$  and  $\delta = 100$  nm.

## References

- 5.1 F. H. Dill, et al., "Characterization of Positive Photoresists," *IEEE Trans. Electron Devices*, Vol. ED-22, No. 7, (July, 1975) pp. 445-452.
- 5.2 M. A. Narasimham and J. B. Lounsbury, "Dissolution Characterization of Some Positive Photoresist Systems," *Semiconductor Microlithography II, Proc.*, SPIE Vol. 100, (1977) pp. 57-64.
- 5.3 C. A. Mack, "Development of Positive Photoresist," *Jour. Electrochemical Society*, Vol. 134, No. 1 (Jan. 1987) pp. 148-152.
- 5.4 C. A. Mack, "New Kinetic Model for Resist Dissolution," *Jour. Electrochemical Society*, Vol. 139, No. 4 (Apr. 1992) pp. L35-L37.

- 5.5 P. Trefonas and B. K. Daniels, "New Principle for Image Enhancement in Single Layer Positive Photoresists," *Advances in Resist Technology and Processing IV, Proc.*, SPIE Vol. 771 (1987) pp. 194-210.
- 5.6 F. H. Dill and J. M. Shaw, "Thermal Effects on the Photoresist AZ1350J," *IBM Jour. Res. Dev.*, Vol. 21, No. 3, (May, 1977) pp. 210-218.
- 5.7 T. R. Pampalone, "Novolac Resins Used in Positive Resist Systems," *Solid State Tech.*, Vol. 27, No. 6 (June, 1984) pp. 115-120.
- 5.8 D. J. Kim, W. G. Oldham and A. R. Neureuther, "Development of Positive Photoresist," *IEEE Trans. Electron Dev.*, Vol. ED-31, No. 12, (Dec., 1984) pp. 1730-1735.
- 5.9 C. A. Mack, D. P. DeWitt, B. K. Tsai, and G. Yetter, "Modeling of Solvent Evaporation Effects for Hot Plate Baking of Photoresist," *Advances in Resist Technology and Processing XI, Proc.*, SPIE Vol. 2195 (1994) pp. 584-595.

# Chapter 6

## Solvent Diffusion Model

In order to simulate solvent evaporation during the baking of a photoresist, two things are required. First, a model for how the diffusivity varies during the bake (that is, as a function of the changing photoresist film composition) must be established. Second, a mathematical technique for solving the diffusion equation must be provided. In this chapter, a historical review of the Fujita-Doolittle equation for solvent diffusivity is given. Then, modifications to this equation are proposed to improve its accuracy and dynamic range. Finally, a numerical technique for solving the diffusion equation in the presence of time-evolving film thickness and properties is presented.

### A. Doolittle's Equation

The influence of temperature, molecular weight, and chemical composition on the physical and mechanical properties of polymers is a difficult but important topic of study. Since the early 1950s the use of a “free-volume” description of physical relaxation phenomena in polymers and other materials has proven extremely useful. Although the idea that the free, unoccupied volume in a liquid or solid greatly influences the physical properties of the material is quite old [6.1], it was first applied successfully by Arthur Doolittle in 1951 [6.2].

Doolittle described the influence of temperature on the viscosity of a liquid in two steps: the viscosity depends on the free volume in the liquid, and this free volume depends on temperature. The fraction of the volume of a liquid which is free, that is, unoccupied by the molecules of the liquid, was expressed by Doolittle as

$$v_f = \frac{V - V_o}{V} \quad (6.1)$$

where  $v_f$  is the free volume fraction,  $V$  is the volume that a specified mass of the liquid occupies at some temperature  $T$ , and  $V_o$  is the volume occupied by the liquid extrapolated to zero absolute temperature assuming no phase change. The assumption here is that the “liquid” extrapolated to absolute zero will contain no free volume and that the thermal expansion of the liquid is due completely to the creation of free volume. Although the first assumption seems quite reasonable, the second is probably less accurate. Thermal expansion of the liquid will undoubtedly lead to free volume formation, but the increased

vibrations of the liquid molecules will also lead to an increased “occupied” volume, the volume that is occupied by the molecule to the exclusion of other molecules. Doolittle’s free volume expression can be modified by multiplying by  $\zeta$ , the fraction of the increased volume which is actually free. Thus,

$$v_f = \zeta \frac{V - V_o}{V} \quad (6.2)$$

where the magnitude of  $\zeta$  is for a liquid is probably close to unity, but for a solid could be considerably smaller.

[Note that other definitions of free volume can and have been used. However, all definitions become the same for the condition of small free volume that is assumed in this work. Thus, no effort will be made to explore the differences in the definitions of free volume.]

The difficulty in measuring the free volume is in determining the value of  $V_o$ . Doolittle attempted this by measuring the density of a liquid as a function of temperature, fitting this data to an empirical equation, then extrapolating to zero temperature. The resulting empirical equation was somewhat cumbersome and non-physical, but fit the data well:

$$\ln\left(\frac{\rho}{\rho_o}\right) = K\left(1 - e^{T/T_1}\right) - \left(\frac{T}{T_2}\right)^n \quad (6.3)$$

where  $\rho$  is the density at temperature  $T$ ,  $\rho_o$  is the density extrapolated to absolute zero, and  $K$ ,  $n$ ,  $T_1$ , and  $T_2$  are empirically determined constants (about 0.1, 1.19, 364K, and 200K, respectively, for the liquid studied). In addition,  $K$  was found to vary inversely with molecular weight for the simple hydrocarbon liquids studied. Density can then be related to free volume using equation (6.2).

$$\frac{\rho}{\rho_o} = 1 - \frac{v_f}{\zeta} \quad (6.4)$$

With this empirically determined temperature dependence for the free volume of the liquid, Doolittle then showed that experimental viscosity data as a function of temperature behaved as

$$\eta = A e^{B/v_f} \quad (6.5)$$

Where  $\eta$  is the viscosity and  $A$  and  $B$  are empirical constants. Equation (6.5) was found to match the experimental data over a wider range of temperatures much better than any of the other empirical expressions in common use at the time, lending credence to this free volume interpretation. Unfortunately, Doolittle did not offer a physical explanation for the form of this equation. Interestingly,

the experimental value of  $B$  obtained by Doolittle was very close to unity (0.9995) and the free volume of the liquid ranged from 0.22 to 0.68 over the temperatures studied.

## B. Temperature Dependence of Free Volume

Others began applying the ideas of free volume to polymer systems. Describing both viscosity and diffusion processes in polymers by the same mechanism, Bueche [6.3] calculated the probability that sufficient free volume would be available to allow movement of the polymer. Relaxation processes (i.e., processes that are limited by the movement of the polymer) were thought to include such phenomenon as viscous flow and diffusion. Thus, describing the rate at which a polymer moved was the first step in defining other relaxation rates. Since the polymer segments are vibrating as a function of temperature, the volume occupied by the polymer will have a thermodynamically controlled probability distribution about the average volume per polymer segment. If the volume occupied by the polymer segment exceeds some critical volume, the polymer segment can move or “jump” to a new configuration. Thus, integrating the volume probability from this critical volume to infinity, the frequency of jumps can be determined. In turn, the viscosity is almost completely controlled by this jump frequency. By comparing this theory with experimental polymer viscosity data, the temperature dependence of the average volume of a polymer segment was deduced. For temperatures above the glass transition temperature of the polymer, Bueche described the polymer volume by [6.3]

$$V = V_{T_g} (1 + (\alpha_1 + \alpha_2)T) \quad (6.6)$$

where  $V_{T_g}$  is the volume at the glass transition temperature,  $\alpha_1$  is the coefficient of thermal expansion of the solid-like polymer below the glass transition temperature, and  $\alpha_1 + \alpha_2$  is the thermal expansion coefficient of the liquid-like polymer above the glass transition temperature. This abrupt change in the coefficient of thermal expansion is considered one of the fundamental indicators of the glass transition phenomenon. Both  $\alpha_1$  and  $\alpha_2$  typically have magnitudes on the order of  $5 \times 10^{-4} \text{ K}^{-1}$  for most polymers. Unfortunately, Bueche’s theory was still not able to explain the success of Doolittle’s viscosity equation (6.5).

Fox and Flory measured the specific volume of polystyrene [6.4] and polyisobutylene [6.5] as a function of temperature for many molecular weights and found that equation (6.6) was quite adequate. Bueche [6.3] and Fox and Flory [6.4] went on to speculate that of the total volume expansion given by equation (6.6), only the  $\alpha_2$  term resulted in the generation of free volume. Essentially, they argued that  $\zeta$  of equation (6.2) was very small for the solid-like behavior of the polymer, and the excess volume that comes from thermal expansion above the glass transition temperature is all free volume. Thus,

$$\begin{aligned} v_f &= v_g, & T &\leq T_g \\ v_f &= v_g + \alpha_2 (T - T_g), & T &\geq T_g \end{aligned} \quad (6.7)$$

where  $T_g$  is the glass transition temperature and  $v_g$  is the fractional free volume at  $T_g$ . Fox and Flory further showed that the specific volume of a polymer is independent of molecular weight below the glass transition temperature [6.4]. Thus, one could conclude from this observation that  $v_g$  is independent of molecular weight and is essentially the same for all polymers. It should be noted, however, that all polymers studied by Fox and Flory were prepared in bulk under similar conditions. It will be shown later that the initial preparation technique may significantly influence the value of  $v_g$ .

The free volume approach to polymer properties was further advanced by Williams, Landel and Ferry. They found empirically that all mechanical and electrical relaxation processes varied with temperature according to a simple, “universal” equation [6.6]. By combining equation (6.7) with Doolittle’s viscosity equation (6.5), the resulting equation matched the Williams, Landel, Ferry (WLF) empirical equation when  $v_g = 0.025$  and  $\alpha_2 = 4.8 \times 10^{-4} \text{ K}^{-1}$ . The equation matched experiment for a wide array of polymer systems over about a 100°C temperature range beginning at the glass transition temperature. The theoretical underpinnings of the WLF equations have been described extensively by Ferry [6.7].

Cohen and Turnbull [6.8] succeeded in providing a theoretical explanation for Doolittle’s equation. Expanding on the work of Bueche, they simplified the probability distribution of the volume occupied by a liquid molecule by assuming a simple, hard sphere description of the liquid. For a liquid molecule occupying a fractional volume  $v^*$  ( $= 1 - v_f$ ), the probability of finding a neighboring hole of size  $v^*$  or larger that the liquid can move into is given by

$$P(v^*) = e^{-\gamma v^*/v_f} = e^\gamma e^{-\gamma/v_f} \quad (6.8)$$

where  $\gamma$  is a statistical correction for overlapping free volume between adjacent molecules and is expected to be between 0.5 and 1. The self diffusion coefficient of such a liquid is then simply proportional to this probability of an available space to move into, and the viscosity of the liquid would be inversely proportional to this probability. Cohen and Turnbull’s simple hard sphere model of the motion of liquids became the first theory to predict Doolittle’s free volume equation (6.5). As a reference point, simple liquids exhibit diffusion coefficients between  $10^{-5}$  and  $10^{-4} \text{ cm}^2/\text{s}$  ( $10^9$  and  $10^{10} \text{ nm}^2/\text{s}$ ).

Another interesting aspect of the Cohen and Turnbull theory is their assumption that no energy is required for the liquid molecule to move into an adjacent hole. Energy is used only in the creation of free volume. Thus, according to this approach, the temperature dependence of diffusion comes only from the temperature dependence of the free volume. In reality, it must take some energy for the liquid to overcome its attraction to its neighbors and move into the free volume. The Cohen and Turnbull assumption, which is used throughout, is that this energy is small compared to the energy requirements of free volume generation. In the context of solvent diffusion through a polymer, it is assumed that diffusion is limited by the availability of free volume so that the interaction of the solvent with the polymer is negligible.

### C. Fujita’s Equation

The power of the free volume approach to relaxation mechanisms is that the fundamental relationship of the relaxation mechanism to free volume is independent of the mechanism by which free

volume changes. Fujita, Kishimoto and Matsumoto [6.9] used this fact to expand the Doolittle and Cohen/Turnbull equations to include the effect of small amounts of solvent in the polymer. Solvent dissolved in a polymer results in additional free volume which in turn increases diffusivity and decreases viscosity. Fujita et al. modified the free volume equation (6.7) to include solvent content:

$$v_f = v_g + \alpha_2 (T - T_g) + \beta \phi_s \quad (6.9)$$

where  $\phi_s$  is the fractional volume of solvent and  $\beta$  describes the fraction of this solvent volume which can be considered free. Here,  $T_g$  is usually considered the glass transition temperature of the completely dry (no dissolved solvent) polymer. For the polymethyl acrylate polymer and four different solvents studied by Fujita et al.,  $\beta$  was found to be 0.19 [6.9].

#### D. Modified Fujita-Doolittle Equation

The Fujita-Doolittle equation has been used extensively to characterize the change in solvent diffusivity with changing solvent concentration. There are, however, constraints to this approach that have led some workers in this field to criticize its use and to look to alternate expressions. In this section, I will address those criticisms and modify the Fujita-Doolittle equation for more general use.

An important point to consider is the temperature range over which equation (6.9) is valid. Equation (6.7) explicitly applies to temperatures above  $T_g$ . Fujita and subsequent authors have simply assumed that equation (6.9) is also restricted in the same way, providing one of the main complaints of the application of the Fujita-Doolittle approach – its limited temperature range. In reality, equation (6.9) can be applied to all temperatures which keep the free volume above  $v_g$ . In other words, whenever,  $v_f > v_g$  the polymer is in its rubbery state and changes in temperature cause linear changes in free volume. When  $v_f$  reaches  $v_g$ , the free volume becomes “frozen” in the polymer and further reduction in temperature does not affect the free volume (or affects it only slightly). Thus, equation (6.9) provides an implicit description of how solvent dissolved in the polymer plasticizes the polymer and lowers its actual glass transition temperature:

$$T_g(\phi_s) = T_g(\phi_s = 0) - \frac{\beta \phi_s}{\alpha_2} \quad (6.10)$$

This new, interesting relationship will be used later to provide simple estimates of  $T_g$  (at  $\phi_s = 0$ ) and  $\beta/\alpha_2$ .

Vrentas, Duda and Ling [6.10] have pointed out that thermal expansion of the solvent also leads to free volume creation. Thus, for a polymer-solvent system with volume fraction  $\phi_p$  of polymer and  $\phi_s$  of solvent ( $\phi_p + \phi_s \approx 1$ , ignoring the small free volume),

$$v_f = \phi_p (v_g + \alpha_{2p} (T - T_{g,p})) + \phi_s (\beta + \alpha_{2s} (T - T_{g,s})) \quad (6.11)$$

where the  $p$  and  $s$  subscripts refer to the respective polymer and solvent properties. Vrentas and Duda have used equation (6.11) to complain that the Fujita-Doolittle approach has too many adjustable parameters and thus other approaches (in particular, their own) should be used.

Fortunately, a simplification of equation (6.11) can be made. First, the temperature  $T_g$  is essentially any convenient reference temperature for assuming a linear increase in free volume with temperature. Thus, no loss in generality occurs when picking the same reference temperature for both polymer and solvent expansion. Next, rearranging this equation,

$$v_f = (1 - \phi_s)v_g + \alpha_2(T - T_g) + \phi_s \beta \quad (6.12)$$

where  $\alpha_2 = \phi_s \alpha_{2s} + \phi_p \alpha_{2p}$  is a volume fraction weighted average of the excess thermal expansion coefficients of the solvent and polymer. However, the WLF equation implies a near-universal behavior of free volume temperature expansion with  $\alpha_{2p} \approx \alpha_{2s} = \alpha_2 = 4.8 \times 10^{-4} \text{ K}^{-1}$ . If this is even close to true, the volume fraction weighted average  $\alpha_2$  can be replaced by a constant value. For example, if the actual values of  $\alpha_{2p}$  and  $\alpha_{2s}$  differ by a factor of 2, then the weighted average  $\alpha_2$  will vary by only  $\pm 5\%$  over a solvent volume fraction range from 0 to 0.2. Equation (6.12) is a more accurate form of the Fujita free volume expression valid for higher concentrations of solvent, while still requiring the same number of parameters as the original free volume expression. It can be thought of as accounting for the dilution of the polymer-induced free volume with the addition of solvent.

The final expression for free volume, equation (6.12), can now be combined with the Doolittle equation to give a modified Fujita-Doolittle equation for the diffusivity of a solvent in a polymer matrix as a function of temperature and solvent content.

$$D = A e^{-B/v_f} \quad (6.13)$$

Letting  $D_o$  be the minimum diffusivity, that is the diffusivity in the limit of no solvent content and  $T = T_g$ ,

$$D_o = A e^{-B/v_g} \quad (6.14)$$

Thus, equation (6.13) can be rearranged as

$$D = D_o e^{-B(1/v_f - 1/v_g)}$$

where 
$$v_f = (1 - \phi_s)v_g + \alpha_2(T - T_g) + \phi_s \beta \quad (6.15)$$

For the experimental data that is used in this work, it will often be more convenient to describe the solvent content as a mass fraction rather than a volume fraction. Letting  $x$  be the mass fraction,  $m$  the mass,  $V$  the volume and  $\rho$  the density,

$$x_s = \frac{m_s}{m_s + m_p} = \frac{V_s \rho_s}{V_s \rho_s + V_p \rho_p} \approx \frac{\rho_s}{\rho_p} \phi_s \left( 1 - \phi_s \left( \frac{\rho_s}{\rho_p} - 1 \right) \right) \quad (6.16)$$

Thus, if either  $\rho_s$  is close to  $\rho_p$ , or  $\phi_s$  is small, then the mass fraction of solvent can be approximated by

$$x_s \approx \frac{\rho_s}{\rho_p} \phi_s \quad (6.17)$$

As an example, if the solvent density is 0.9 and the polymer density is 1.1, then less than a 5% error will be made by applying equation (6.17) up to a solvent fraction of 0.275. Thus, equation (6.15) can be modified to use the mass fraction of solvent:

$$D = D_o e^{-B(1/v_f - 1/v_g)}$$

where  $v_f = (1 - x_s)v_g + \alpha_2(T - T_g) + x_s \beta'$

and  $\beta' = \frac{\rho_p}{\rho_s} \beta + v_g \left( 1 - \frac{\rho_p}{\rho_s} \right) \approx \frac{\rho_p}{\rho_s} \beta \quad (6.18)$

Equation (6.18) is the modified Fujita-Doolittle equation that is used in this work and is shown in Figure 6-1 for typical parameters.

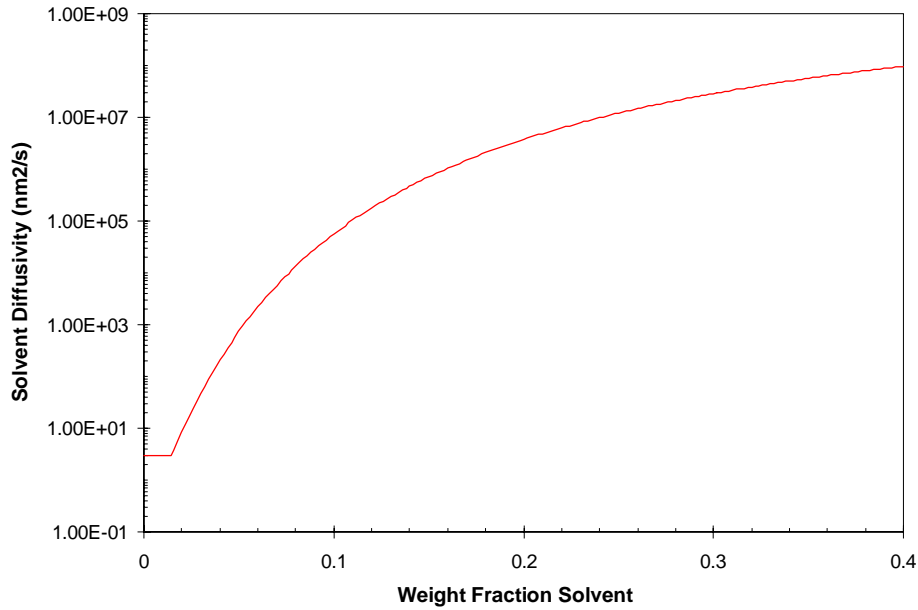


Figure 6-1. Plot of the modified Fujita-Doolittle equation for  $A = 1.10 \times 10^{10} \text{ nm}^2/\text{s}$ ,  $B = 0.737$ ,  $\beta' = 0.351$ ,  $v_g = 0.0335$ ,  $\alpha_2 = 8.68 \times 10^{-4}$ ,  $T_g = 110.5^\circ\text{C}$ , evaluated at a temperature of  $105^\circ\text{C}$ . Below  $x_s = 0.02$ , the polymer becomes glassy and the diffusivity remains constant.

### E. Estimating Parameters in the Modified Fujita-Doolittle Equation

Based on previous work, the order of magnitude for each of the terms in equation (6.18) is known. Doolittle [6.2] and Williams, Landel and Ferry [6.6] found  $B$  to be approximately 1.0, while Fujita et al. [6.9] found  $B = 0.73$ . Cohen and Turnbull [6.8] limit  $B$  to be between 0.5 and 1 (their so-called geometric factor). The WLF equation predicts  $v_g = 0.025$  and  $\alpha_2 = 4.8 \times 10^{-4} \text{ K}^{-1}$  [6.6], but further work by Ferry [6.7] found values of  $v_g/B$  between 0.013 and 0.07, with most of the data between 0.02 and 0.035, and values of  $\alpha_2$  between 1 and  $11 \times 10^{-4} \text{ K}^{-1}$ , with most data between 3 and  $5 \times 10^{-4} \text{ K}^{-1}$ . Fox and Flory [6.4] found  $\alpha_2 = 3 \times 10^{-4} \text{ K}^{-1}$ . Fujita found  $\beta$  to be 0.19, and in any case it must be  $\leq 1.0$ . The value of  $\beta'$  should be similar.

Equation (6.10) describing the plasticizing effects of solvent on the polymer can be used to provide estimates of  $T_g$  (at  $\phi_s = 0$ ) and  $\beta/\alpha_2$ . When baking a thin film of polymer to drive out solvents, if the bake time is of the same order as typical  $T_g$  measurements (i.e., on the order of tens of minutes to an hour), the final film will reach that non-equilibrium state where further relaxation (diffusion of solvent) is very slow. In other words, the  $T_g$  of the resulting film will be equal to the bake temperature. If the final average solvent content of the film can be measured for different bake temperatures  $T_b$ , estimates of  $T_g$  (at  $x_s = 0$ ) and  $\beta/\alpha_2 - v_g$  can be made from

$$x_{s,avg} = \frac{T_g - T_b}{\frac{\beta'}{\alpha_2} - v_g} \quad (6.19)$$

Further, since the thickness of the final film is approximately linear with  $x_{s,avg}$ , a plot of thickness versus bake temperature will give

$$\frac{\beta'}{\alpha_2} - v_g - T_g \approx \frac{y - \text{intercept}}{\text{slope}} \quad (6.20)$$

## F. Solving the Diffusion Equation

One can predict the solvent content in a photoresist after a post apply bake by solving the standard diffusion equation in one dimension:

$$\frac{\partial C_s}{\partial t} = \frac{\partial}{\partial z} \left( D \frac{\partial C_s}{\partial z} \right) \quad (6.21)$$

where  $C_s$  is the concentration of solvent and  $D$  is the diffusivity of solvent in photoresist. Solving this equation requires a number of things: two boundary conditions, one initial condition, and a knowledge of the diffusivity as a function of position and time.

The initial condition is the initial solvent distribution within the film,  $C_s(z,0)$  and, implicitly, the initial film thickness. When fitting the quartz crystal microbalance (QCM) desorption experimental data in Chapter 7, the initial condition will simply be a uniform solvent concentration. The two boundary conditions are at the top and bottom surface of the photoresist film. The boundary at the substrate surface is assumed to be impermeable, giving a boundary condition of no diffusion into the substrate. The boundary condition at the top of the wafer will depend on the diffusion of evaporated solvent in the atmosphere above the wafer. In general, one can assume that the diffusivity of solvent in air is significantly higher than in resist. Thus, if the volume of air above the wafer (or the air flow rate) is sufficiently large, solvent which escapes the resist surface will immediately dissipate into the environment, leaving an atmospheric solvent concentration at the top of the photoresist film of zero. For the desorption experiments carried out in a vacuum as described in Chapter 7, this assumption is certainly true. This is equivalent to saying that the diffusion process is controlled by internal resistance within the film, rather than by the rate of evaporation. This boundary condition is quite reasonable as long as the sample is not in a small closed container with limited airflow.

The solution of equation (6.21) can now be performed if the diffusivity of the solvent in the photoresist is known. Unfortunately, this solution is complicated by two very important factors: the diffusivity is a strong function of temperature and of solvent concentration. The temperature and concentration dependence of diffusivity is described with the modified Fujita-Doolittle expression (6.18).

Since the solvent concentration is time and position dependent, the diffusivity in equation (6.21) must be determined as a part of the solution of equation (6.21) by an iterative method.

One of the most common iterative approaches to solving the diffusion equation is the finite difference time domain (FDTD) method [6.11]. In this technique, the differential equation (6.21) is replaced by a difference equation. Beginning with the initial condition  $C_s(z, 0)$ , the difference equation is used to calculate the spatial distribution of solvent after some small time step  $\Delta t$ . At each time step, the new solvent distribution results in a new diffusivity of the solvent as given by the modified Fujita-Doolittle equation. Marching through time until the end of the bake, the final solvent distribution is determined.

One important consideration in the FDTD approach is the convergence criterion. In order for this iterative method to converge properly to the correct solution, certain stability requirements are placed on the choice of the spatial and temporal increments of the iterations. Let us define the incremental diffusion length as the average distance a molecule of solvent diffuses in one iterative time step:

$$\Delta\sigma = \sqrt{2D\Delta t} \quad (6.22)$$

The convergence requirement is that the spatial increment  $\Delta z$  must be less than or equal to about  $3\Delta\sigma$ . Thus, given a spatial increment chosen to provide the desired resolution in the final solvent distribution, the time increment can be chosen by

$$\Delta t = \frac{\Delta z^2}{18D} \quad (6.23)$$

The FDTD solution is complicated considerably by the fact that solvent evaporation changes the thickness of the film. If the film is initially broken up into uniform increments of thickness  $\Delta z$ , each incremental thickness will contain the same amount of solvent. Over time, however, solvent evaporation will change the solvent content of each thickness increment differently. As a result, the thickness of each increment will evolve with time. To compute this changing increment thickness, some basic relationships can be used. The concentration of solvent is related to the weight fraction solvent by

$$C_s = x_s \rho_{film} \quad (6.24)$$

where  $\rho_{film}$  is the overall density of the thickness increment in question. The film density is assumed to obey a linear mixing rule of volumes:

$$\rho_{film} = \left( \frac{x_s}{\rho_s} + \frac{1-x_s}{\rho_p} \right)^{-1} = \rho_p + C_s \left( 1 - \frac{\rho_p}{\rho_s} \right) \quad (6.25)$$

The change in thickness with changing solvent content can be determined by realizing that the mass of polymer ( $m_p$ ) in each thickness increment does not change. Using the subscript  $i$  to denote the initial condition,

$$m_p = \Delta z_i \rho_{film,i} (1 - x_{s,i}) \quad (6.26)$$

Then, at any time increment the current thickness increment will be

$$\Delta z = \frac{m_p}{\rho_{film} (1 - x_s)} \quad (6.27)$$

The final FDTD solution uses the following calculations: 1) For the current time step and current  $C_s$ , calculate  $\rho_{film}$  and  $x_s$  and  $\Delta z$  for every thickness increment using equations (6.24), (6.25), and (6.27) and calculate the solvent diffusivity for each thickness increment using the modified Fujita-Doolittle equation (6.18). 2) Determine the required time increment from the convergence criterion (6.23) using the maximum diffusivity within the film. 3) Using these values for  $\Delta t$ ,  $\Delta z$  and  $D$ , apply the FDTD update equations to get the value of  $C_s$  at the next time increment.

In the next chapter, this solution approach is used to match the solvent diffusion model to experimental data.

## References

- 6.1 A. J. Batschinski, *Z. Physik Chem.*, Vol. 84 (1913) p. 644.
- 6.2 A. K. Doolittle, "Studies in Newtonian Flow. II. The Dependence of the Viscosity of Liquids on Free-Space," *Journal of Applied Physics*, Vol. 22, No. 12 (Dec., 1951) pp. 1471-1475.
- 6.3 F. Bueche, "Segmental Mobility of Polymers Near Their Glass Temperature," *Journal of Chemical Physics*, Vol. 21, No. 10 (Oct., 1953) pp. 1850-1855.
- 6.4 T. G. Fox and P. J. Flory, "Second-Order Transition Temperatures and Related Properties in Polystyrene. I. Influence of Molecular Weight," *Journal of Applied Physics*, Vol. 21 (Jun., 1950) pp. 581-591.
- 6.5 T. G. Fox and P. J. Flory, "Further Studies on the Melt Viscosity of Polyisobutylene," *Journal of Physical and Colloid Chemistry*, Vol. 55 (1951) pp. 221-234.
- 6.6 M. L. Williams, R. F. Landel, and J. D. Ferry, "The Temperature Dependence of Relaxation Mechanisms in Amorphous Polymers and Other Glass-forming Liquids," *Journal of the American Chemical Society*, Vol. 77 (Jul. 20, 1955) pp. 3701-3706.
- 6.7 J. D. Ferry, *Viscoelastic Properties of Polymers*, 3<sup>rd</sup> edition, John Wiley and Sons (New York: 1980).
- 6.8 M. H. Cohen and D. Turnbull, "Molecular Transport in Liquids and Gases," *Journal of Chemical Physics*, Vol. 31, No. 5 (Nov., 1959) pp. 1164-1169.
- 6.9 H. Fujita, A. Kishimoto, and K. Matsumoto, "Concentration and Temperature Dependence of Diffusion Coefficients for Systems Polymethyl Acrylate and n-Alkyl Acetates," *Transactions of the Faraday Society*, Vol. 56 (1960) pp. 424-437.
- 6.10 J. S. Vrentas, J. L. Duda, and H.-C. Ling, "Free-Volume Theories for Self Diffusion in Polymer-Solvent Systems. I. Conceptual Differences in Theories," *Journal of Polymer Science*, Vol. 23 (1985) pp. 275-288.
- 6.11 F. P. Incropera and D. P. DeWitt, *Fundamentals of Heat and Mass Transfer*, 3<sup>rd</sup> edition, John Wiley & Sons (New York: 1990).

# Chapter 7

## Comparison of Solvent Diffusion Model to Measurements

Comparison of a model to experiment can be used to both confirm the validity of the model and to extract the necessary modeling parameters. For the case of solvent diffusion modeling, experimental measurement of the amount of solvent remaining in a photoresist film as a function of bake time and temperature is required. Two separate techniques have been used to measure the amount of residual casting solvent in a photoresist: the quartz crystal microbalance (QCM) [7.1] and liquid scintillation counting (LSC) of radio-labeled solvent [7.2]. Matching of this data to the model proposed in Chapter 6 will provide valuable insight into the solvent diffusion process and allow extraction of the model parameters for the photoresist studied.

### A. Quartz Crystal Microbalance

One of the most common techniques for measuring solvent diffusion in polymers is to weigh a sample of the polymer as solvent diffuses out, then solve the diffusion equation for the boundary conditions of the experiment and extract the diffusivity by a fit of this solution to the data [7.3]. Although large bulk samples of polymer allow the use of conventional mass measurements, diffusion through thin films requires special techniques for measurement of the small mass changes involved.

The piezoelectric property of crystalline quartz allows this material to be used as an electromechanical transducer and as a highly stable oscillator for frequency control. A quartz crystal oscillator can also be used as a sensing device for measuring the thickness of thin films deposited on the quartz, since a shift in resonant frequency is proportional to the deposited mass [7.4]:

$$\Delta f = \frac{-2f_o^2 \Delta m}{A\sqrt{\mu_Q \rho_Q}} \quad (7.1)$$

where  $\Delta f$  is the frequency change,  $f_o$  the resonant frequency of the resonator before this change (nominally 6 MHz),  $\Delta m$  the change in mass,  $A$  the piezoelectrically active area ( $1.04 \pm 0.02 \text{ cm}^2$ ),  $\rho_Q$  the density of the quartz ( $2.648 \text{ g/cm}^3$ ), and  $\mu_Q$  the shear modulus of AT-cut quartz ( $2.947 \times 10^{11} \text{ dyne/cm}^2$ ).

One of the most attractive features of a quartz crystal microbalance (QCM) is that the frequency can be precisely measured to 1 part in  $10^{10}$ , resulting in very precise measurements of the change in mass. For our purposes, the adsorption or desorption of solvent from a photoresist film coated on a QCM can be measured as a change in mass of the film.

Experiments were performed by means of an apparatus that is shown in Figure 7-1 [7.1]. The photoresist chosen for study was AZ9100 (Clariant Corp., Somerville, NJ), which uses a solvent of propyleneglycol methyl ether acetate (PGMEA) at about 38 wt% solids. The PGMEA has a density of 0.966 g/ml and the dry photoresist has a density of about 1.1 g/ml. Quartz crystals with polished gold electrodes were coated with the resist film by spin coating at 2500 RPM for 30 seconds and hotplate baking at 90°C for 90 seconds, resulting in about 4.5  $\mu\text{m}$  thick films.

The resist coated crystals were inserted into the crystal holder and vacuum was applied until there was no measurable change in the frequency, indicating a stable film. The entire system was maintained at a constant temperature of 50, 70, 90 or 100°C  $\pm$  0.3°C by circulating a water/ethylene glycol mixture through the double-walled sample chamber and the water lines that lead to the crystal holder. The portion of the apparatus that was not heated by the circulating fluid was maintained at a constant temperature through the use of heating tape and insulation. Solvent, which is maintained at the same constant temperature by another heating bath, was then introduced into the chamber, and solvent uptake was observed by monitoring the decrease in crystal frequency, indicating an increase in mass. Once the absorption of solvent by the film was complete (indicated by a constant crystal frequency, typically after about 10 minutes of exposure to the vapor), the solvent supply was closed, the system evacuated and a desorption run was carried out. Thus, the measured output for the desorption experiment was the mass of the film as a function of time, giving a direct measurement of the amount of solvent diffusing out of the film.

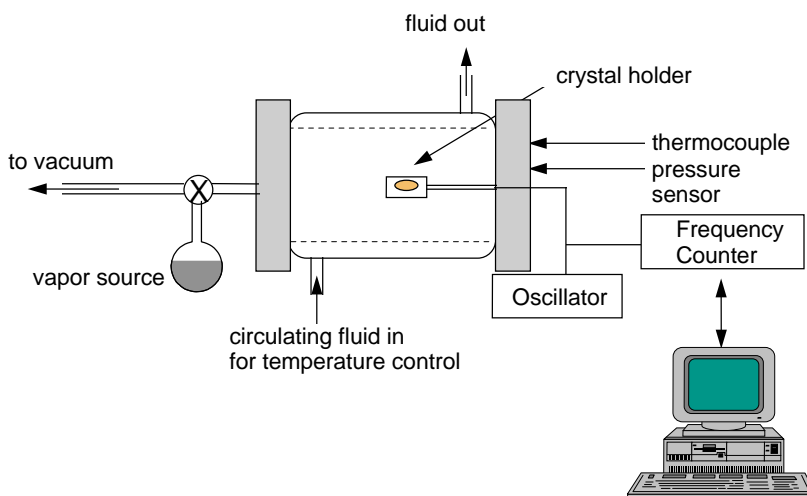


Figure 7-1. Quartz Crystal Microbalance (QCM) in an environmentally controlled chamber was used to measure the diffusion of solvents in a photoresist film [7.1].

Figure 7-2 shows an example of the output produced by this experiment. The mass loss of the film at time  $t$ , given by  $M_t$ , is shown relative the final mass loss at the end of the experiment, designated

as  $M_\infty$ . Although only the first 10,000 seconds (2.78 hours) of data are shown in Figure 7-2, data collection continued for a total of 14.4 hours at 90°C, 50.5 hours at 70°C, and for 65.9 hours at 50°C. The kinetics of thermal decomposition of the photoactive compound used for this resist are known to produce insignificant amounts of decomposition for the times and temperatures used in this study. Thus, it was assumed that all of the mass loss measured could be attributed to loss of solvent.

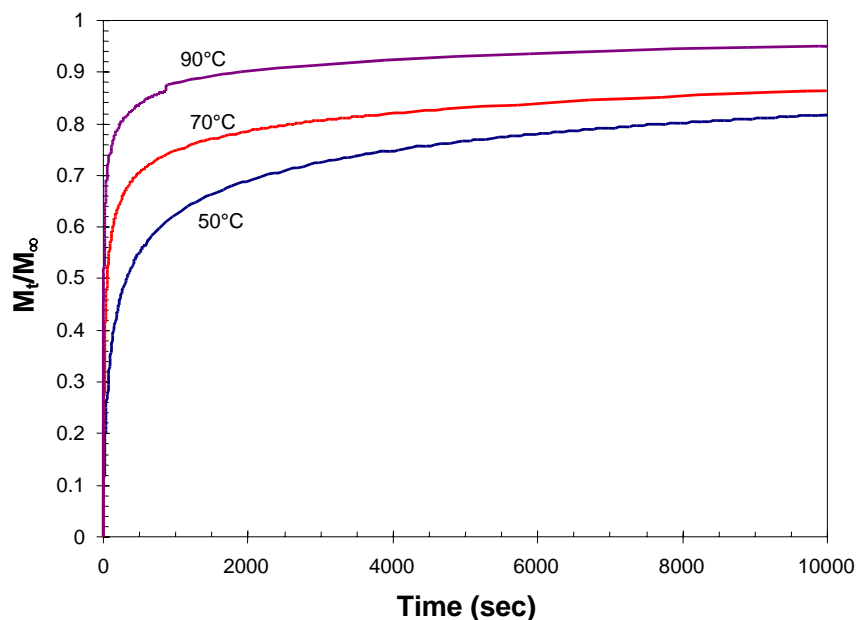


Figure 7-2. Solvent desorption from an AZ9100 resist film at 50, 70 and 90°C, represented as a fractional weight loss ( $M_t/M_\infty$ ) [7.5].

## B. Liquid Scintillation Counting

The total amount of residual casting solvent in a resist film after post apply bake (PAB) can be measured by scintillation counting of a radio-labeled solvent [7.2]. This method provides the most direct means of determining solvent content in resist films. For this study, the solvent was radio-labeled with  $^{14}\text{C}$  and the radioactivity of the solvent and resist film was analyzed using a Beckman 1801 liquid scintillation counter and Fisher ScintiVerse II scintillation cocktail.

Radio-labeled solvent was first used to calibrate the QCM measurements described above. For each temperature studied, resist laced with the radio-labeled solvent was coated on a quartz crystal and subjected to the desorption experiment in the QCM apparatus. The crystal was then removed and the final weight percent of solvent remaining was determined by liquid scintillation counting (LSC) [7.6]. The results are shown in Table 7-1. Once an absolute value for the final solvent content was determined, the initial solvent content was calculated using the data from Figure 7-2 and equation (7.1). In addition, final resist thickness was measured using a reflectance spectrophotometer (using Cauchy coefficients of the refractive index measured for each sample with a spectroscopic ellipsometer). These results are also given in Table 7-1. From the data in this table, and using equations (6.25) and (6.27), the initial film thickness was estimated to be 6.67, 6.90, and  $6.58 \pm 0.17$   $\mu\text{m}$  for the 50, 70 and 90 °C trials, respectively.

Table 7-1: Measured final solvent content and film thickness  
for the data shown in Figure 7-2.

Temperature (°C)	Initial Solvent (wt%)	Final Solvent (wt%)	Final Thickness (microns)
50	38.3 ± 1.0	16.7 ± 0.3	4.80 ± 0.02
70	37.3 ± 1.0	12.8 ± 0.3	4.80 ± 0.02
90	36.0 ± 0.8	9.0 ± 0.3	4.46 ± 0.02

In a second experiment, resist solutions were spin coated on 4 inch silicon wafers, varying the spin speed for each baking temperature to produce film thicknesses close to 4.5µm. Several different baking times were used at each hotplate PAB temperature of 90°C, 105°C, and 115°C ± 0.5°C (the recommended PAB temperatures for this resist are between 105 and 115°C). Exactly 2 minutes after finishing the PAB, the film was dissolved with 5 mL of non-radio-labeled casting solvent and then 14 mL of scintillation cocktail. During this 2 minute delay period the films were cooled for 15 seconds, the thickness was measured, and the coated wafer was weighed. Figure 7-3 shows the results of this experiment. The error in the LSC measurements was estimated to be ±0.3 wt%.

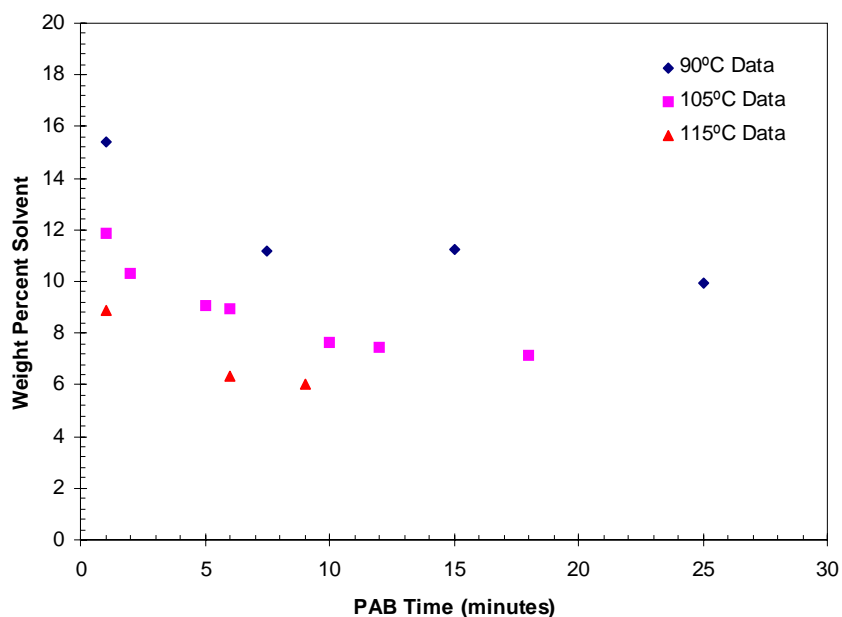
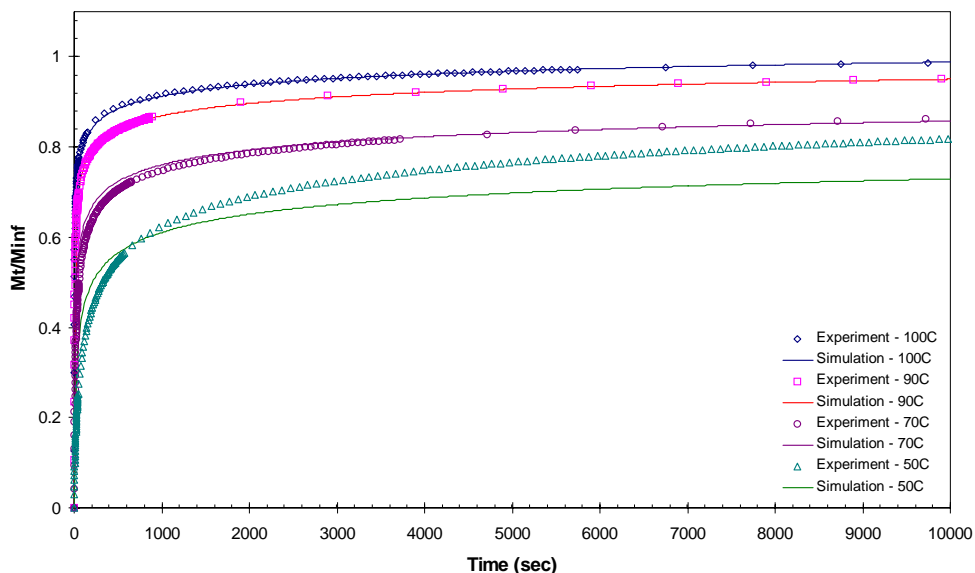


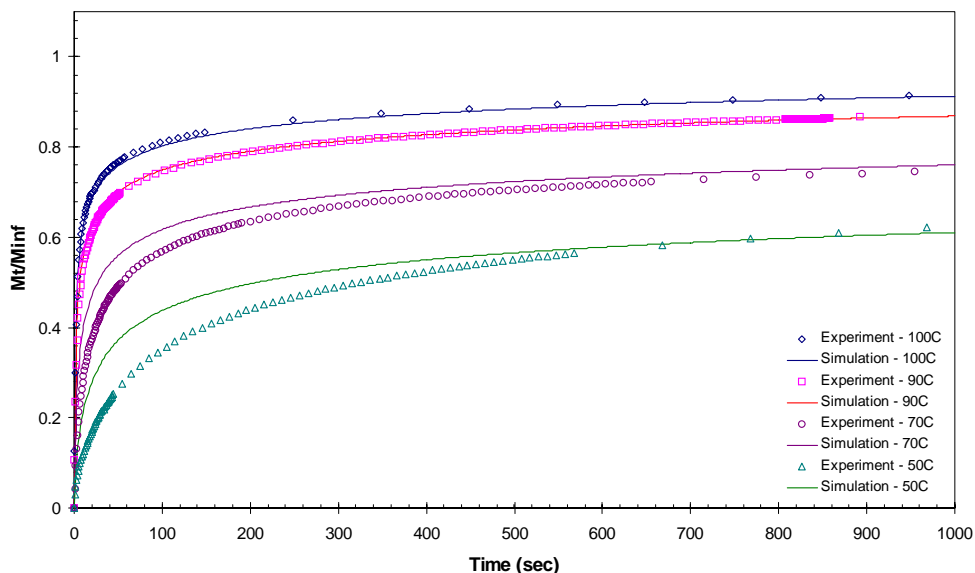
Figure 7-3. Measured weight percent solvent in resist (coated on a silicon wafer) after post apply bake as a function of PAB time and temperature [7.2].

### C. Comparison of Diffusion Model to QCM Data

The modified Fujita-Doolittle model proposed in Chapter 6 was implemented in a software program using the finite difference time domain approach with variable grid spacing. The unknown parameters of equation (6.18) were adjusted to obtain the best match of the model to the experimental QCM measurements. The initial conditions were taken to be a thickness of  $6.7\mu\text{m}$  and 37wt% solvent for all temperatures. Figure 7-4 shows the results of this effort, the three graphs representing three different time scales. As can be seen, excellent agreement is seen for the 90°C and 100°C data over all time scales, with the match getting worse as the temperature is lowered.



(a)



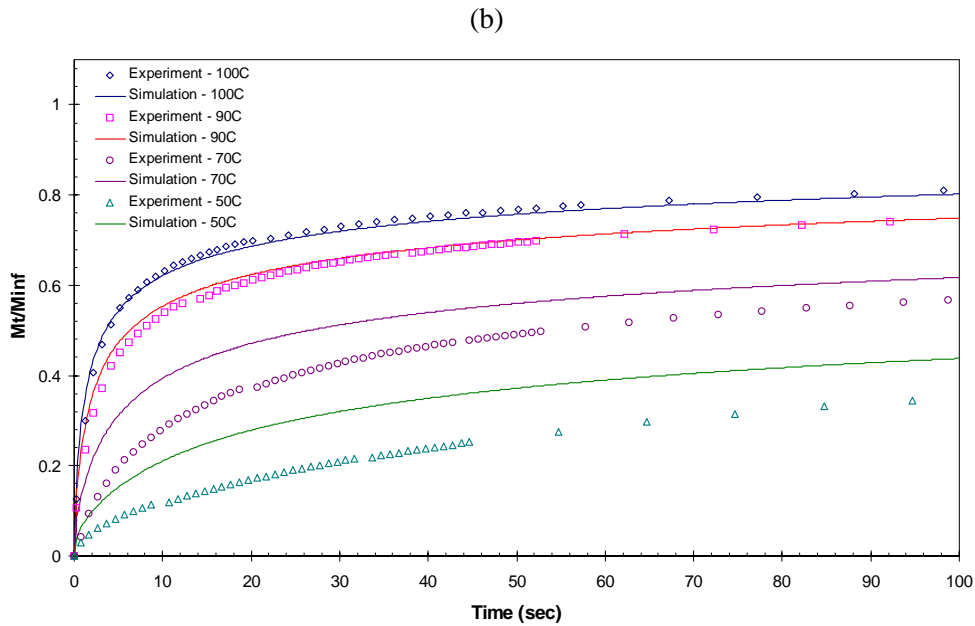


Figure 7-4. Comparison of the diffusion model with QCM data [7.5], plotted on (a) long, (b) moderate and (c) short time scales to better show the nature of the match.

The 70°C temperature data matches well over the long time scale, but less well for the shorter times. The 50°C temperature data shows significant deviation from the model, but since this temperature is far outside the useful range of post apply bake temperatures, this deviation was not considered important. It is also important to note that range of times shown in these figures is quite large. It is a very strict test of the model to match the experimental data over short, moderate and long time scales simultaneously.

#### D. Comparison of Diffusion Model to LSC Data

The situation is more complicated when trying to match the spin coat liquid scintillation counting (LSC) data of Figure 7-3 as well as the QCM data using the same parameter set. The difference between the two data sets lies in their initial conditions. The QCM films were spin coated, but then were kept at the elevated bake temperature while solvent saturated the film (the saturation bake). As a result, the initial condition is a simple uniform solvent distribution. Further, the saturation bake anneals the polymer film, allow some portion of the free volume generated by the high-stress spin coat process to be relaxed. Thus, the LSC process differs from the QCM process in two ways: a different initial solvent distribution and a different value of  $v_g$ .

The solvent model can be used to examine the impact of different initial conditions. After extensive simulations a very interesting trend emerged. Any combination of initial resist thickness and initial solvent content that produced a certain final resist thickness always resulted in essentially the same solvent distribution in the resist. Thus, by matching the initial conditions to provide the desired final resist thickness, a unique solvent distribution result is insured. In the case of the LSC data, the spin speed

during coating was adjusted for each bake temperature. Thus, the initial resist thickness/initial solvent content would be different for each bake. To determine the required initial conditions, the calculated final resist thickness was compared to the measured final resist thickness. As shown in Figure 7-5, good correlation was obtained by assuming an initial solvent content of 30 wt% and initial resist thicknesses of 5.55, 6.00 and 6.32  $\mu\text{m}$  for the 90, 105, and 115°C bake conditions, respectively.

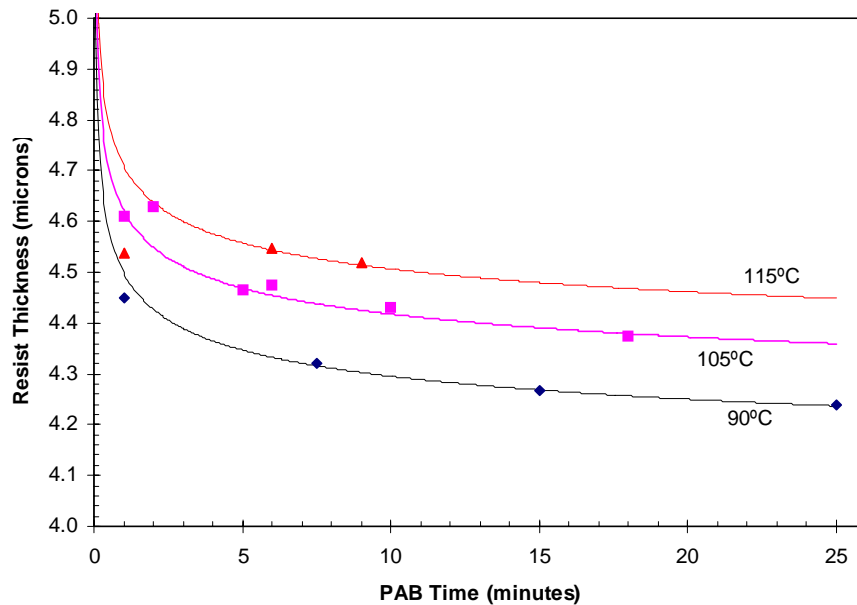
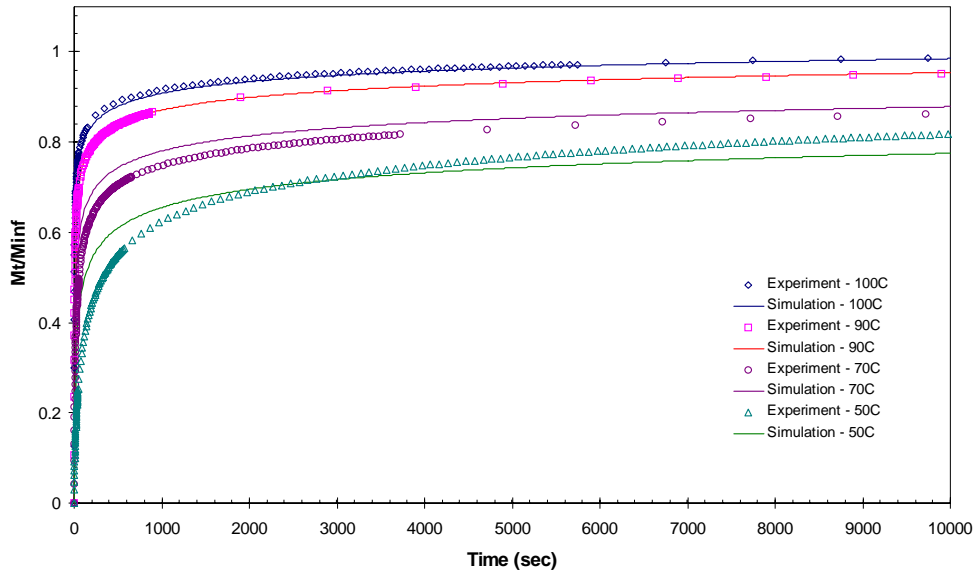
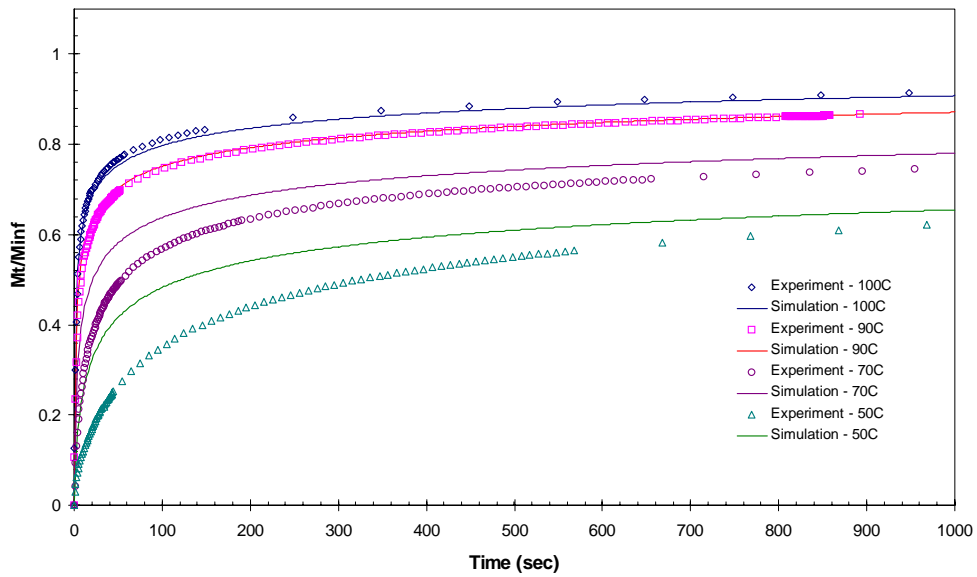


Figure 7-5. Comparison of the diffusion model (lines) with resist thickness data (symbols) in order to determine the spin coat initial conditions.

Further attempts to match the experimental data were made by allowing only  $v_g$  to vary between the QCM and LSC data sets. The results are shown in Figures 7-6 and 7-7, using the parameters in Table 7-2. As can be seen, the model still fits well to the QCM data at 90°C and 100°C, but the fit to the lower temperature data has worsened. The fit to the LSC data is good at all temperatures.



(a)



(b)

Figure 7-6. Comparison of the diffusion model with QCM data [7.5], plotted on (a) long and (b) moderate time scales.

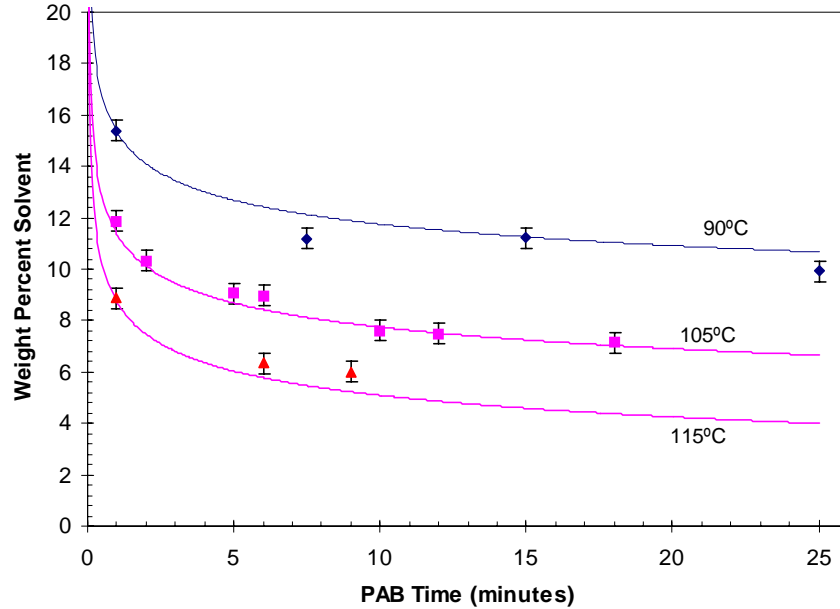


Figure 7-7. Comparison of the diffusion model (lines) with LSC data (symbols) [7.6].

Table 7-2: Best fit model parameters for the data in Figures 7-2 and 7-3.

Parameter	Best Fit Value	Parameter Uncertainty (100 sec fit)	Parameter Uncertainty (10,000 sec fit)
$B$	0.737	$\pm 0.005$	$\pm 0.010$
$\beta'$	0.351	$\pm 0.004$	$\pm 0.004$
$\nu_g$ (QCM)	0.0289	$\pm 0.0001$	$\pm 0.0002$
$\nu_g$ (Spin Coat)	0.0335	$\pm 0.0001$	$\pm 0.0002$
$\alpha_2$ (1/K)	8.7E-04	$\pm 0.3E-04$	$\pm 0.2E-04$
$T_g$ ( $^{\circ}\text{C}$ )	110.5	$\pm 0.7$	$\pm 0.5$
$A$ ( $\text{nm}^2/\text{s}$ )	1.15E+10	$\pm 0.12E+10$	$\pm 0.15E+10$

Errors in the values of the parameters extracted from the data in general arise from two sources: the goodness of the fit and the errors intrinsic to the raw data. In the case of the LSC data and the 90 and 100°C QCM data, the errors due to the goodness of fit (or the lack thereof) are small compared to the errors in the data itself. All of the data, even the QCM data, is limited by the accuracy of the LSC

calibration, estimated to be  $\pm 3\%$ . Thus, the uncertainty in the values of the extracted parameters can be estimated by assuming the raw data exhibits a  $\pm 3\%$  uncertainty.

Two error estimates were obtained based on the uncertainty in the QCM data. The first estimate was made by fitting only the first 100 seconds of the QCM data and the second estimate used a fit to the 500 - 10,000 second range of the data. The error estimates were obtained by finding the range of each parameter that kept the fit within  $\pm 3\%$  of the data. Then, assuming independence of error sources, the resulting range of each parameter was divided by  $\sqrt{6}$ , corresponding to the six parameters. The results are presented in Table 7-2. As can be seen, some parameters have more or less sensitivity for the short time versus the long time results. The uncertainty for each parameter over the entire range of time can be estimated as the minimum value of the two uncertainties from Table 7-2.

## **E. Using the Model**

The modified Fujita-Doolittle model proposed in Chapter 6 has been compared to quartz crystal microbalance and radio labeled liquid scintillation counting data for a commercial novolac-based photoresist. The results show that the model can accurately predict the resist thickness and solvent distribution at the end of a post apply bake as a function of bake conditions over a wide range of bake temperatures and times.

One important consequence of such a calibrated solvent diffusion model is the ability to predict the solvent distribution as a function of depth into the photoresist (Figure 7-8). Such results can be useful when predicting various resist properties that are a function of solvent content, such as acid diffusivity in a chemically amplified resist or resist dissolution rate. Of course, such solvent distribution plots can be generated for a wide variety of post apply bake times and temperatures.

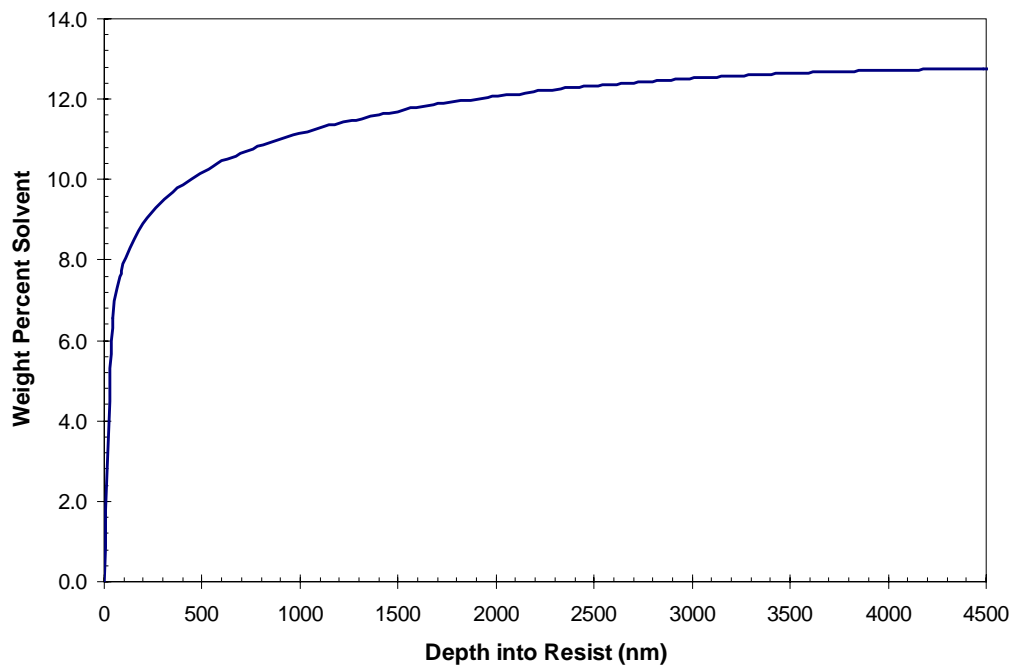


Figure 7-8. Prediction of the solvent distribution within the photoresist after a 60 second, 105°C post apply bake.

## References

- 7.1 K. E. Mueller, W. J. Koros, Y. Y. Wang, and C. G. Willson, "Diffusivity Measurements in Polymers, Part 3: Quartz Crystal Microbalance Techniques," *Advances in Resist Technology and Processing XIV, Proc.*, SPIE Vol. 3049 (1997) pp. 871-878.
- 7.2 Allen B. Gardiner, Anwei Qin, Clifford L. Henderson, William J. Koros, C. Grant Willson, Ralph R. Dammel, Chris Mack, William D. Hinsberg, "Diffusivity Measurements in Polymers, Part 2: Residual Casting Solvent Measurement by Liquid Scintillation Counting," *Advances in Resist Technology and Processing XIV, Proc.*, SPIE Vol. 3049 (1997) pp. 850-860.
- 7.3 K. Imre, "A Quick Method for Determining the Diffusion Coefficient for Polymer-Monomer Systems from Desorption Data," *Journal of Polymer Science: Polymer Chemistry*, Vol. 18 (1980) pp. 1647-1650.
- 7.4 Sauerbrey, G., *Z. Phys. Chem.*, **155**, (1959) pp. 206.
- 7.5 QCM data measured and provided by Kathi Mueller.
- 7.6 LSC data measured and provided by Allen Gardiner.

# Chapter 8

## Summary and Conclusions

The importance of optical lithography to semiconductor technology has resulted in significant work over the last 30 years devoted to studying the fundamental underlying physical and chemical mechanisms of the lithography process. Simulation is one embodiment of this knowledge where the physical and kinetic equations of imaging, diffusion, and chemistry are coded in software. Proper application of such models to real lithographic problems requires three things: an accurate description of the underlying physical principles in a mathematical form, a numerical approach to solving these equations, and numerical values for the physical and chemical parameters used by the model.

Of all the technology areas currently implemented in lithographic modeling software, by far the weakest area is the modeling of the post apply bake step. This step in the lithographic process is meant to drive off residual casting solvent left from the photoresist spin coat step and make the film dry and stable for subsequent patterning. The properties of the remaining film are critical to the performance of the resist. In particular, the solvent remaining in the film after the post apply bake can affect the diffusion of resist components during the post exposure bake and the dissolution rate of the photoresist during development. Thus, an accurate prediction of the solvent distribution from the top to the bottom of the resist film is necessary for accurate modeling of subsequent process steps. Also, the ability to predict how this solvent distribution changes with post apply bake conditions would be of great value.

The goal of this work is to create a model of the lithographic post apply bake process in order to accurately predict the solvent distribution within the photoresist film as a function of bake conditions. Three major accomplishments have been made toward this goal: 1) A new model of solvent diffusivity as a function of bake temperature and solvent concentration has been developed; 2) A numerical calculation algorithm employing a dynamically changing grid has been used to solve the diffusion equation; 3) The resulting model has been calibrated using a commercial resist process and the necessary parameters for accurate simulation have been extracted.

The first accomplishment of this work is the establishment of a new, more accurate model for the temperature and concentration dependence of the solvent diffusivity. Although the Fujita-Doolittle model for solvent diffusivity has been used extensively over the years, it is limited in its range of applicable temperatures and concentrations. Theoretical analysis of the derivation of the Fujita-Doolittle equation has shown that a proper understanding of the application of the model allows its use over an extended temperature range, including temperatures below the glass transition temperature of the polymer. A modification to the Fujita-Doolittle equation was then made that extends its applicability to higher solvent

concentrations. The resulting modified Fujita-Doolittle equation can be applied over a wide enough range of temperatures and solvent content to make this model applicable to solvent diffusion during post apply bake.

The second accomplishment of this work is the variable grid finite difference time domain (FDTD) solution to the diffusion equation. As solvent diffuses out of the thin photoresist film, the film densifies and shrinks. Any spatial grid used for the FDTD computation will then change with time. An approach was devised based on calculation cells of constant polymer content. As solvent diffuses out of a given cell, the cell shrinks in thickness. Thus, the grid can be recomputed for each time step in the FDTD calculation. The result is a robust software program that quickly and accurately solves the diffusion equation under the highly dynamic conditions involved in solvent diffusion and evaporation during post apply bake.

The third accomplishment of this work is the calibration of the model for an example photoresist system. Using a commercial novolac-based resist with PGMEA solvent, solvent content measured with a quartz crystal microbalance (QCM) and with liquid scintillation counting (LSC) of radio-labeled solvent was used to calibrate the model. Resist thickness data provided the information required to establish the initial conditions of the diffusion simulations. Solvent content as a function of time and temperature of the bake was used to calibrate the modified Fujita-Doolittle parameters. The resulting calibrated model accurately reproduced the experimental data over a 30°C range of bake temperatures and over three orders of magnitude of bake time. One parameter in particular, the dry polymer free volume  $v_g$ , was found to be sensitive to the method of film preparation. The high stress conditions of spin coating result in higher amounts of free volume “frozen” into the polymer.

The result of this work, a physically-based, calibrated model of solvent diffusion during post apply bake, can now be applied to a wide range of lithographic problems. The solvent distribution within the photoresist is thought to affect the diffusion, and thus amplification, of acid during the post exposure bake of chemically amplified resists. Solvent content also affects dissolution rate and could explain one source of surface inhibition during development. In such cases, the availability of an accurate model for solvent diffusion is a necessary prerequisite for further work.